

## RESEARCH ARTICLE

10.1002/2017TC004489

## Key Points:

- Extensional pattern changes to a complex compartmentalization dominated by shortening
- Recent inversion of the Alboran Ridge and partial strike-slip reactivation the Yusuf fault
- Controlling factors: fault orientation with respect to the plate convergence; original dips and geometries; fluid content, sedimentary thicknesses, and magmatic intrusions

## Correspondence to:

P. Martínez-García,  
p.martinezgarcia@hw.ac.uk;  
pedromatez@gmail.com

## Citation:

Martínez-García, P., Comas, M., Lonergan, L., & Watts, A. B. (2017). From extension to shortening: Tectonic inversion distributed in time and space in the Alboran sea, western Mediterranean. *Tectonics*, 36, 2777–2805. <https://doi.org/10.1002/2017TC004489>

Received 24 JAN 2017

Accepted 11 SEP 2017

Accepted article online 18 SEP 2017

Published online 4 DEC 2017

# From Extension to Shortening: Tectonic Inversion Distributed in Time and Space in the Alboran Sea, Western Mediterranean

Pedro Martínez-García<sup>1</sup> , Menchu Comas<sup>2</sup> , Lidia Lonergan<sup>3</sup> , and Anthony B. Watts<sup>4</sup> 

<sup>1</sup>Institute of Petroleum Engineering, Heriot-Watt University, Edinburgh, UK, <sup>2</sup>Instituto Andaluz de Ciencias de la Tierra (CSIC and University of Granada), Armilla, Granada, Spain, <sup>3</sup>Department of Earth Science and Engineering, Imperial College London, London, UK, <sup>4</sup>Department of Earth Sciences, University of Oxford, Oxford, UK

**Abstract** 2D seismic reflection data tied to biostratigraphical and log information from wells in the central and southeastern Alboran Sea have allowed us to constrain the spatial and temporal distribution of rifting and inversion. Normal faults, tilted basement blocks, and growth wedges reveal a thinned continental crust that formed in response to NW-SE extension. To the east, a secondary SW-NE trend of extension affects the transitional crust adjacent to the oceanic Algerian Basin. The maximum thickness of syn-rift sediments is ~3.5 km, and the oldest recorded deposits are Serravallian. The WNW-ESE Yusuf fault formed a buttress separating and accommodating variable extension between two different tectonic domains: the thinned continental crust of Alboran and the oceanic spreading of the Algerian Basin. Late Tortonian to present-day NW-SE Africa/Eurasia plate convergence drove shortening and reactivation of some of the earlier extensional structures as reverse and strike-slip faults, forming complex, compartmentalised subbasins. Tectonic inversion coexisted with the formation of new faults and folds. Inversion was partial along the Habibas Basin and Al-Idrisi fault, but complete along the Alboran Ridge, where some SW-NE trending faults were perpendicular to the recent NW-SE plate convergence and were reactivated as thrusts. The WNW-ESE Yusuf fault is oblique to the convergence vector, and therefore, reactivation is mainly expressed as transpressional deformation. Volcanic rocks intruded along the Alboran Ridge and Yusuf faults during the latest stages of extension formed rheological anisotropies that localised the later inversion.

## 1. Introduction

Positive tectonic inversion refers to the contractional or transpressional reactivation of normal faults inherited from an earlier tectonic phase due to a change in the tectonic regime from crustal extension to shortening. Fault reactivation is often highly selective and only occurs along some fault segments of a preexisting fault network. The slip is preferentially partitioned along segments with favourable orientation with respect to the applied compressional stresses resulting in either dip-slip or strike-slip displacements (e.g., Hayward & Graham, 1989; Jones et al., 2004; Turner & Williams, 2004). Other factors controlling inversion are (1) the existence of rheological anisotropies in the basement, (2) the presence of low-friction material along faults, and (3) the heterogeneous distribution of fluid overpressures (e.g., Marques & Nogueira, 2008; Sibson, 1995). Inversion structures have been widely studied due to their role as traps for hydrocarbons, and they have been recognised in different geodynamic settings including amongst others: orogenic belts such as the Zagros, the Alps, the Rocky Mountains, and the Andes (e.g., Butler, 1989; Carrera et al., 2006; Jackson, 1980; McClay & Anderton, 1989); rift systems in East Africa and the North Sea (e.g., Jackson & Larsen, 2008; Le Gall, Vétel, & Morley, 2005); and back-arc basins such as the Sea of Japan and the Black Sea (e.g., Munteanu et al., 2011; Takano, Tateishi, & Endo, 2005).

In the Mediterranean, several extensional basins formed during the Miocene due to the collapse of Alpine orogens at ~25–30 Ma and were later partially inverted and deformed under a transpressional regime within a convergent tectonic setting between the African and Eurasian plates (e.g., Cloetingh et al., 2008; Faccenna et al., 2004; Gallais et al., 2011; Giaconia et al., 2015; Horvath & Berckhemer, 1982; Rosenbaum, Lister, & Duboz, 2002; Strzeczynski et al., 2010). The westernmost of these basins is the Alboran Sea, which experienced folding, reverse and strike-slip faulting, and uplift of basin margins during the Plio-Quaternary (e.g., Alvarez-Marrón et al., 1999; Bourgois et al., 1992; Comas, García-Dueñas,

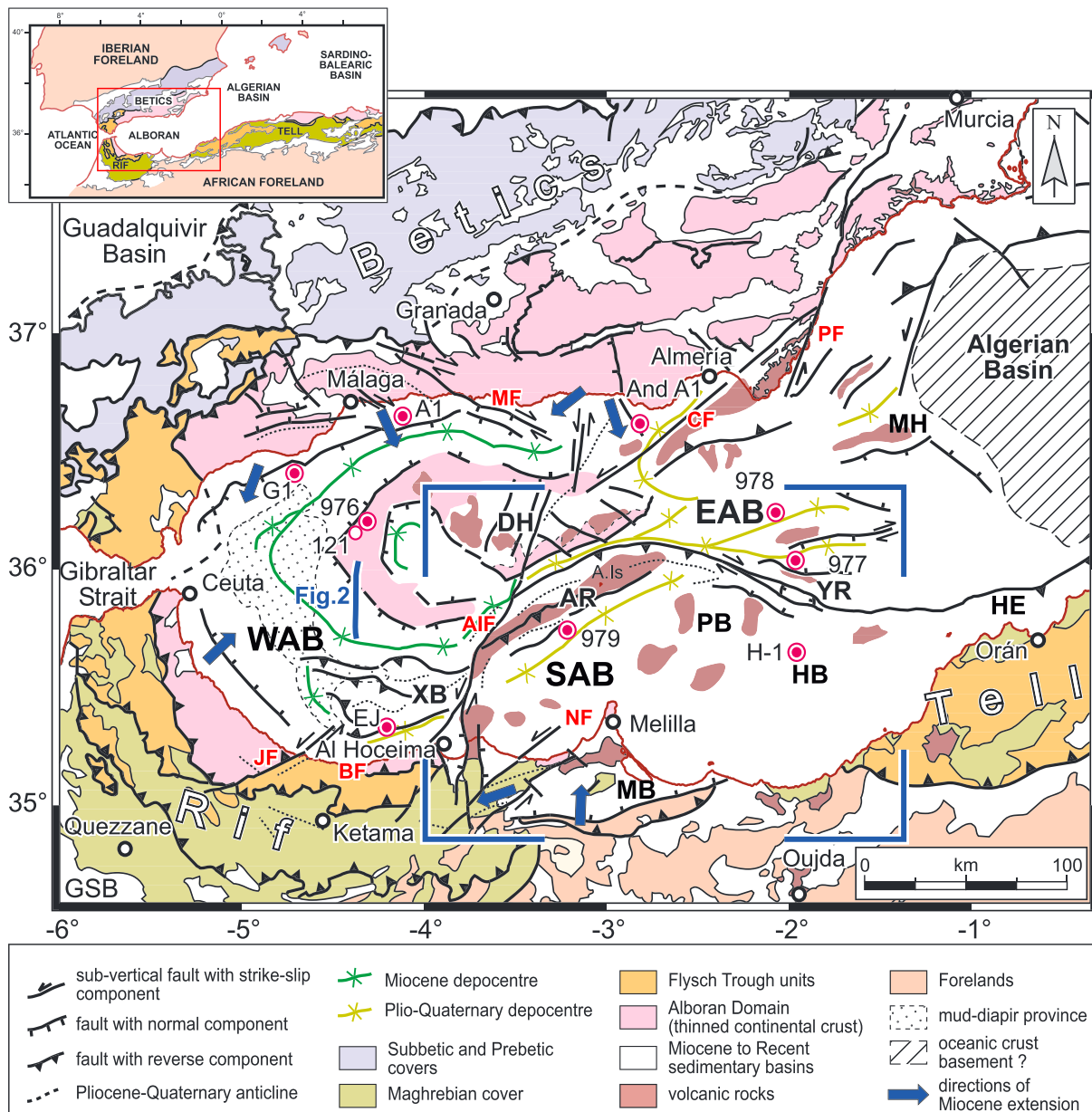


**Figure 1.** Geological map of the Alboran Sea Basin and surrounding areas showing early Miocene to Holocene structures and main sedimentary depocentres (after Martínez-García et al., 2011 and Do Couto et al., 2016). The rectangle marks the study area. The blue arrows are directions of Miocene extension (Azzimousa et al., 2007; Booth-Rea et al., 2012; Comas et al., 1999; Martínez-Martínez et al., 2004). The red circles are ODP leg 161 sites (976 to 979), DSDP site 121, and commercial boreholes (G1: Andalucía-G1, A1: Alboran-A1, and A1: Andalucía-A1, EJ: El-Jebha, and H-1: Habibas-1). The inset map shows main tectonic elements in the western Mediterranean. Abbreviations: A. Is, Alboran Island; AIF, Al-Idrisi fault; AR, Alboran Ridge; BF, Bokkoya Fault; CF, Carboneras Fault; DH, Djibouti High; EAB, East Alboran Basin; GSB, Gharb-Saïss Basin; HB, Habibas Basin; HE, Habibas Escarpment; JF, Jebha Fault; MB, Melilla Basin; MF, Maro-Nerja Fault; MH, Maimonides High; NF, Nekor Fault; PB, Pytheas Basin; PF, Palomares Fault; SAB, South Alboran Basin; XB, Xauen Bank; YR, Yusuf Ridge; WAB, West Alboran Basin.

& Jurado, 1992; Chalouan et al., 1997; Comas et al., 1999; Docherty & Banda, 1995; Mauffret et al., 2007; Woodside & Maldonado, 1992) (Figure 1).

The extensional history of the Alboran Sea Basin has been widely studied in its western and northern sectors and also throughout its remnants within the surrounding Betics and Rif, where its continental crustal basement crops out widely, and it is deformed by numerous normal faults and detachments (e.g., Azzimousa et al., 2007; Benmakhoulouf et al., 2012; Booth-Rea et al., 2012; Chalouan et al., 2008;

Comas et al., 1999; García-Dueñas, Balanyá, & Martínez-Martínez, 1992; Maldonado et al., 1992; Platt et al., 1998; Platt & Vissers, 1989; Watts, Platt, & Buhl, 1993). However, little is known about the rifting geometry in the central and southeastern parts of the basin where a significant number of Plio-Quaternary structures are found (e.g., Mauffret et al., 2007; Medaouri et al., 2014). Additionally, the role of preexisting Miocene faults during the shortening phase is still unclear. Whether these structures were reactivated and localised compressive deformation remains to be determined.

The aims of this study are to (1) reconstruct the deep structure of the basin to better constrain the Miocene extensional evolution and understand how the inherited structural pattern influenced the distribution of deformation during the postrift shortening stages and (2) determine the timing and factors controlling the inversion.

## 2. Geological Setting

The Alboran Sea Basin, in the western Mediterranean, is a major extensional basin surrounded by an Alpine orogenic belt, which comprises the Betic and Rif mountain chains and an accretionary wedge in the Gulf of Cadiz. The whole system is known as the Gibraltar Arc System and was formed during the Neogene by simultaneous outward thrusting in the frontal parts of the surrounding mountain belts and extensional collapse in the inner part of the arc within a general setting of plate convergence between the African and Eurasian plates (e.g., Comas et al., 1992, 1999; Dewey, 1988; García-Dueñas et al., 1992; Jolivet & Faccenna, 2000; Lonergan & White, 1997; Platt & Vissers, 1989; Rosenbaum et al., 2002; Watts et al., 1993). Several pre-Neogene crustal domains were involved in the formation of this orogen (Figure 1).

The Alboran Domain constitutes the thinned continental basement beneath the Alboran Sea Basin and outcrops largely onshore forming the internal Betics and Rif. During the early to middle Miocene, this continental domain, which was originally located at the south of the Balearic Islands, extended and collided with the Iberian and African passive continental margins. The Subbetic, Prebetic, and Maghrebian paleo-margins and the deep marine flysch clastic deposits were deformed by thin-skinned thrusting and folding as consequence of the emplacement of the Alboran Domain (e.g., Andrieux, Fontbote, & Mattauer, 1971; Balanyá & García-Dueñas, 1987; Frizon de Lamotte, Andrieux, & Guézou, 1991; García-Dueñas et al., 1992; Lonergan, Platt, & Gallagher, 1994). This event produced shortening of the peripheral belt accompanied by the development of the external flexural foreland basins of Guadalquivir and Gharb-Saïss (Figure 1). At the same time, crustal extension occurred in the Alboran Domain by means of normal faulting resulting in the formation of the Alboran Basin (e.g., Galindo-Zaldívar, González Lodeiro, & Jabaloy, 1989; García-Dueñas et al., 1992; Platt & Vissers, 1989). Extensional deformation ceased by the late Tortonian (i.e., ~9–8 Ma, late Miocene) (e.g., Chalouan et al., 1997). Magmatism and volcanism occurred during this rifting event (e.g., Duggen et al., 2004; Hoernle et al., 1999; Turner et al., 1999). Volcanic and subvolcanic rocks are particularly abundant in the central and eastern parts of the Alboran Sea (Figure 1) (Galdeano et al., 1974; Willet, 1997). Early Miocene extension was followed by thermal cooling of the hot asthenosphere producing subsidence (e.g., Docherty & Banda, 1995; Hanne, White, & Lonergan, 2003). Thus, thermal subsidence superimposed on tectonic subsidence resulted in creation of a thermal sag basin in the western Alboran Sea, forming a major curved depocentre (e.g., Do Couto et al., 2016; Morley, 1993). The origin of crustal extension and thinning are still under debate, and several tectonic models have been proposed, which can be grouped into three main hypotheses: (1) postorogenic collapse caused by convective removal of the lithospheric root (e.g., Molnar & Houseman, 2004; Platt & Vissers, 1989); (2) delamination of lithosphere (e.g., Calvert et al., 2000; García-Dueñas et al., 1992; Seber et al., 1996); and (3) subduction zone rollback beneath the Alboran Domain (e.g., Faccenna et al., 2004; Gutscher et al., 2002; Lonergan & White, 1997; Royden, 1993).

Significant thickness variations of the sedimentary cover indicate that both Miocene extension and later shortening were syn-sedimentary processes that compartmentalized the basin into three main subbasins: the West Alboran Basin (WAB), East Alboran Basin (EAB), and South Alboran Basin (SAB). The WAB contains the major depocentre, which is thicker than 8.5 km (Soto, Comas, & de la Linde, 1996; Weinzapfel et al., 2003) (Figures 1 and 2). Towards the east, the sedimentary cover thins to 2–2.5 km in the EAB and 3 km in the SAB (Alonso & Maldonado, 1992; Mauffret et al., 2007).

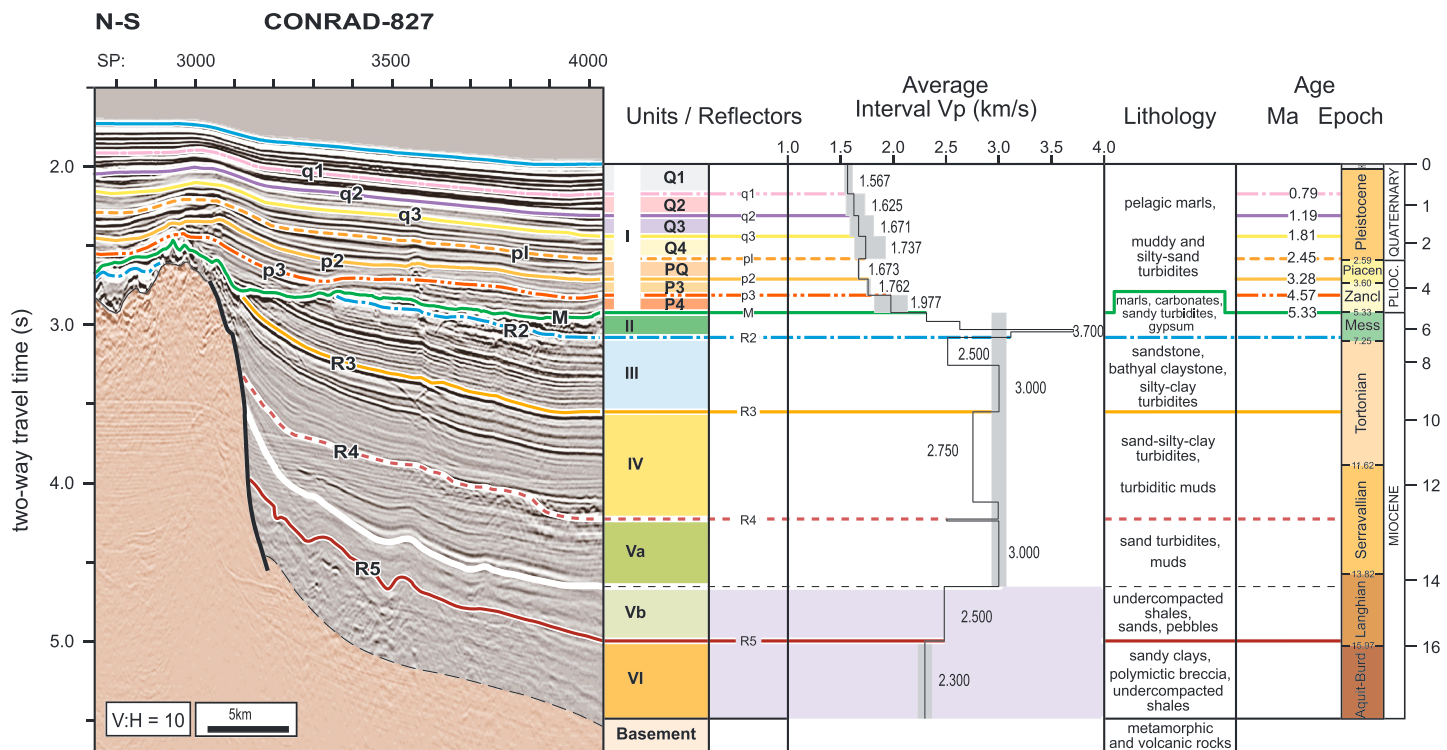


**Figure 2.** Multichannel seismic line showing the seismostratigraphy of the WAB (see location in Figure 1) and correlation with interval sonic velocities ( $V_p$ ), lithology, and ages obtained from ODP sites and commercial wells (Comas et al., 1999; Medaouri et al., 2014). Main seismic units and major reflectors as defined by Jurado and Comas (1992). Plio-Quaternary seismic units, reflectors, and interval  $V_p$  calculated from ODP sites 976 to 979 are taken from Martínez-García et al. (2013). Interval  $V_p$  for the Miocene sequences are taken from Talukder (2003) and came from the commercial well Andalucía-G1. The thick grey bars in the  $V_p$  panel highlight the values used for depth conversions. The purple band marks overpressured shales (units Vb and VI).

### 3. Data and Methodology

A dense grid of 135 seismic reflection profiles totalling 7,790 km, acquired by both academic institutions and the hydrocarbon industry, is used for this study. Single-channel and multichannel seismic (MCS) data cover an area of 28,000 km<sup>2</sup> in the central and southeastern parts of the Alboran Sea Basin (Figures 1 and 3). Some 4,200 km of profiles were vintage analogue records, and they have been scanned and transformed to the standard segy format using Lynx<sup>®</sup> software. Unpublished academic MCS profiles, acquired during the Tecalb and Marsibal I-06 cruises (BIO Hesperides, 2000 and 2006), are used in the figures of this paper and provide new insights supporting our main interpretations. Other academic seismic profiles come from the Conrad cruise C2911 (R/V Robert D. Conrad, 1988) and the Darwin cruise CD 64 (RSS Charles Darwin 1991–1992). The industry data were mainly acquired by Sonatrach (1974), Compagnie Generale de Geophysique (1975), and Eniessa (1979).

For the seismic mapping, events were correlated with well records from DSDP Site 121; ODP Sites 976, 977, 978, and 979; and the commercial Habibas-1 well (Figure 3) (de Kaenel, Siesser, & Murat, 1999; Kheidri, Benabdelmounen, & Zazoun, 2000; Mauffret, 2007; Medaouri et al., 2014; Siesser & de Kaenel, 1999). Detailed chronostratigraphic and log information available for the last ~5 Ma and good resolution of seismic data in the shallower parts of the profiles allowed us to clearly recognize several Plio-Quaternary seismic units and bounding discontinuities. However, seismic resolution decreases in depth and biostratigraphical information is less precise for deposits below a prominent event of Messinian age known as the M reflector (Figure 2). Therefore, the Miocene sedimentary units and unconformities were only locally mapped, and their age attributions should be considered tentative. Time-contour maps (in two-way travel time, twtt) were obtained for the different mapped unconformities by gridding. Time-thickness maps were then calculated for the Plio-Quaternary and Miocene sequences and converted to depth (isopach maps) using average sonic velocities ( $V_p$ ) from Martínez-García et al. (2013) and Talukder (2003) (Figure 2). In addition, we converted some interpreted sections to depth to estimate the magnitudes of extension and shortening using line-length restoration analyses.



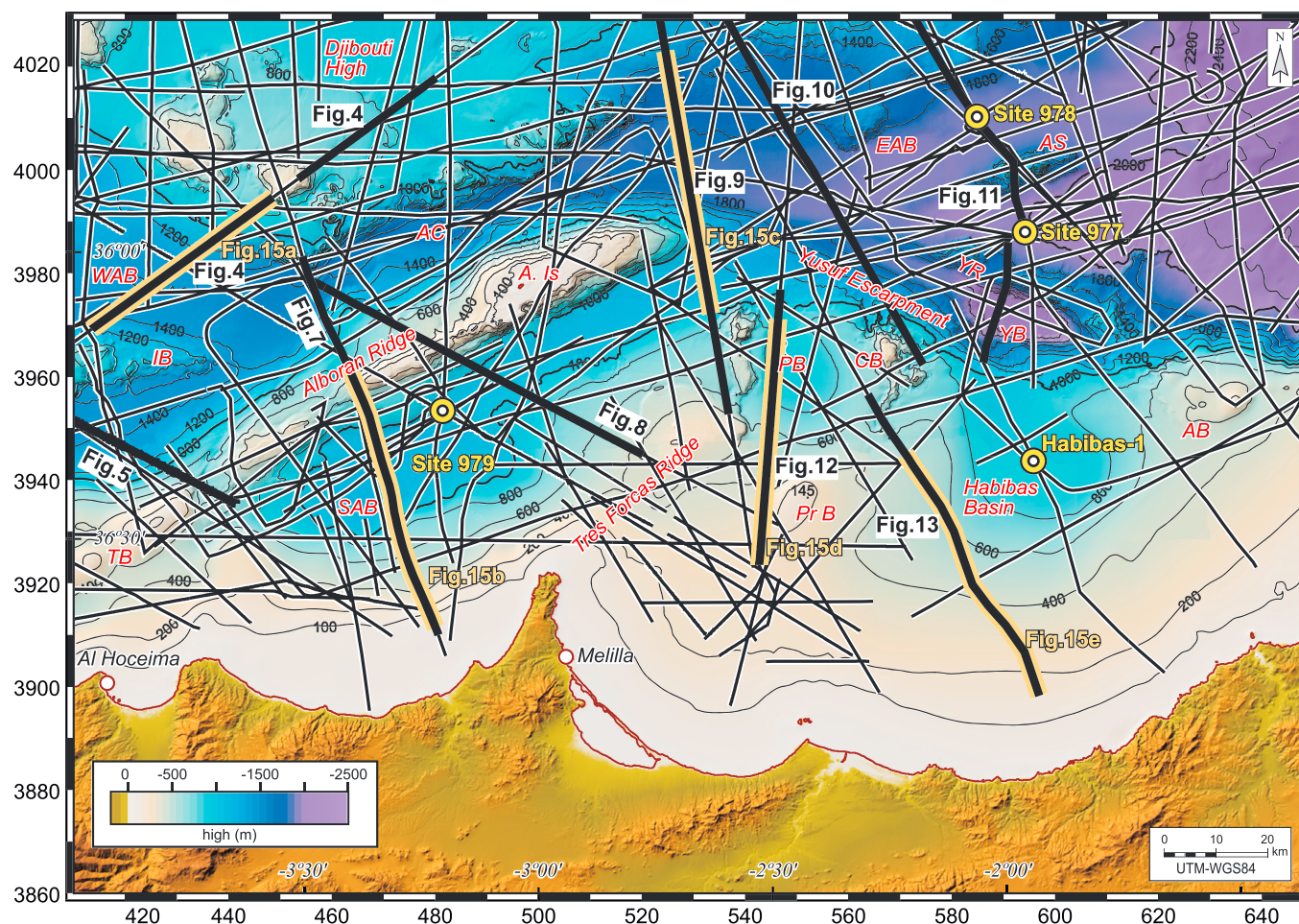


**Figure 3.** Location map showing bathymetry and position of seismic profiles. The thick black lines indicate multichannel seismic profiles presented in other figures. The thick brown segments show location of depth-converted seismic interpretations in Figure 15. Locations of ODP leg 161 sites 977, 978, 979, and Habibas-1 well are also included. Bathymetry is taken from Martínez-García et al. (2011) and combined with digital topography extracted from the SRTM (USGS-NASA) global database. Contour interval is 200 m. UTM projection and units in kilometres. Abbreviations: A. Is, Alboran Island; AB, Alidade Bank; AC, Alboran Channel; AS, Al-Mansour Seamount; CB, Câbliers Bank; EAB, East Alboran Basin; IB, Ibn-Batouta Bank; PB, Pytheas Basin; Pr B, Provençaux Bank; SAB, South Alboran Basin; TB, Tofño Bank; YB, Yusuf Basin; YR, Yusuf Ridge; WAB, West Alboran Basin.

## 4. Seismic Interpretation and Mapping

### 4.1. Seismic Stratigraphy

The seismic horizons we have mapped through the studied region in the Alboran Sea are consistent with the previously published seismostratigraphy (Chalouan et al., 1997; Do Couto et al., 2016; Jurado & Comas, 1992) (Figure 2). Six major units (I to VI) are commonly differentiated, and major seismic discontinuities are labelled following Comas et al. (1999) (R5 to R2 and M). In addition, we also use the Plio-Quaternary seismic subunits and bounding key reflectors defined within Unit I by Martínez-García et al. (2013) (q1 to p3), which are in agreement with the post-Messinian stratigraphy established by Juan et al. (2016) on a regional basin scale. Age attributions and nomenclature have been updated according to the current chronostratigraphic time scale of the International Commission on Stratigraphy (Cohen et al., 2013). The Plio-Quaternary deposits (Unit I) were drilled by ODP Leg 161 and consist of pelagic marls, muddy turbidites, and rare silty-sandy turbidites (Alonso et al., 1999). The base of this unit is a strong erosional unconformity recognized throughout the Mediterranean and known as the M reflector (Hsü, Ryan, & Cita, 1973; Ryan et al., 1973). The event truncates late Miocene deposits and basement on the basin margins and highs but changes laterally into a conformable event into the main depocentres (e.g., Figures 4 and 5). In the deeper parts of the basin, the M reflector marks the Miocene-Pliocene boundary coinciding with the Messinian salinity crisis event at



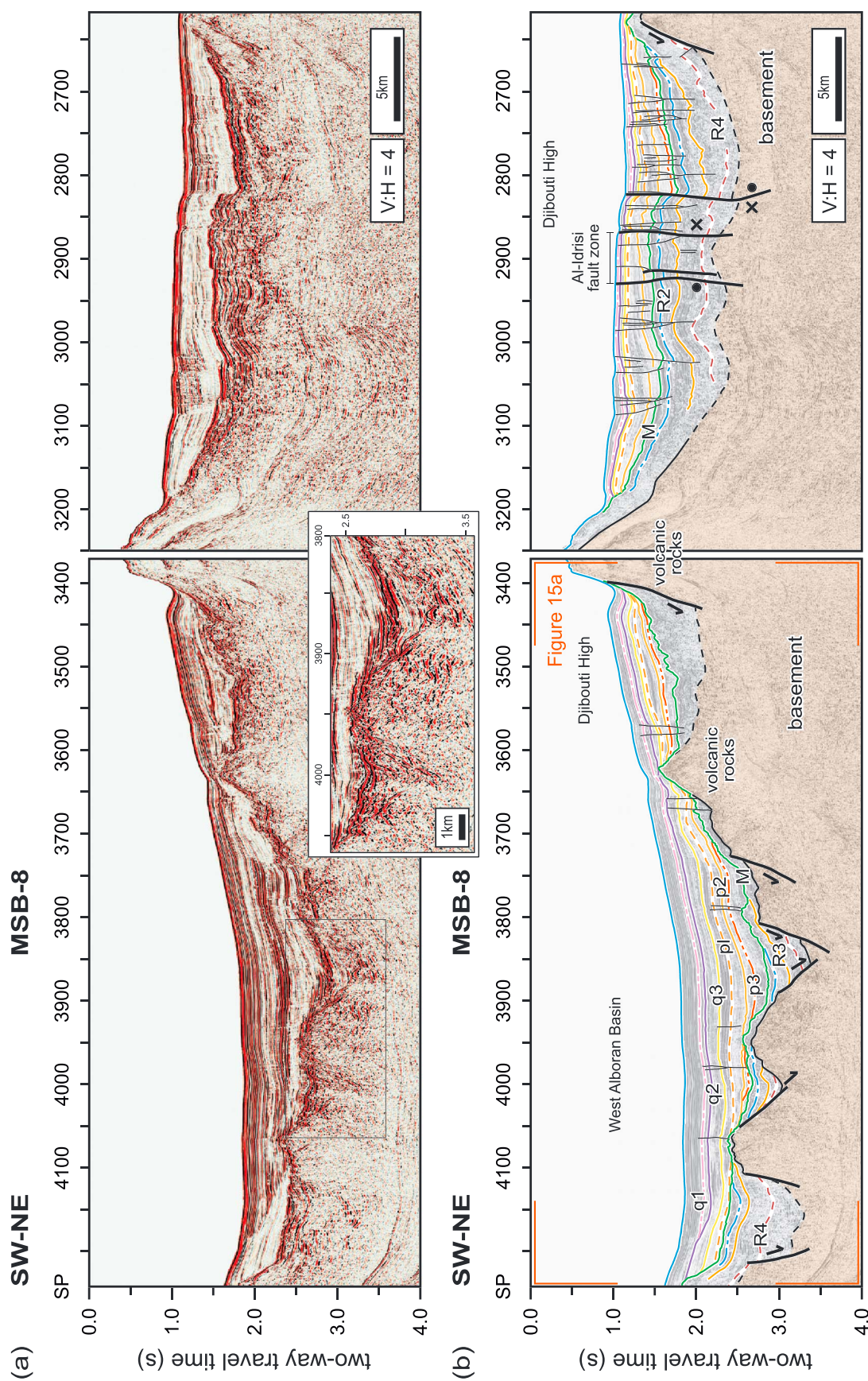


**Figure 4.** (a) Uninterpreted and (b) interpreted multichannel seismic section across the West Alboran Basin (WAB) and the Djibouti High. The R5 to q1 reflectors, age of unconformities, and seismic units are correlated with those defined by Jurado and Comas (1992) for the Miocene sequences (below the M-reflector) and by Martínez-García et al. (2013) for the Plio-Quaternary sequences. Note that Plio-Quaternary deposits seal Miocene extensional structures in the WAB. The dashed lines indicate tentative position of top of basement. The location of seismic line is shown in Figures 3 and 6.

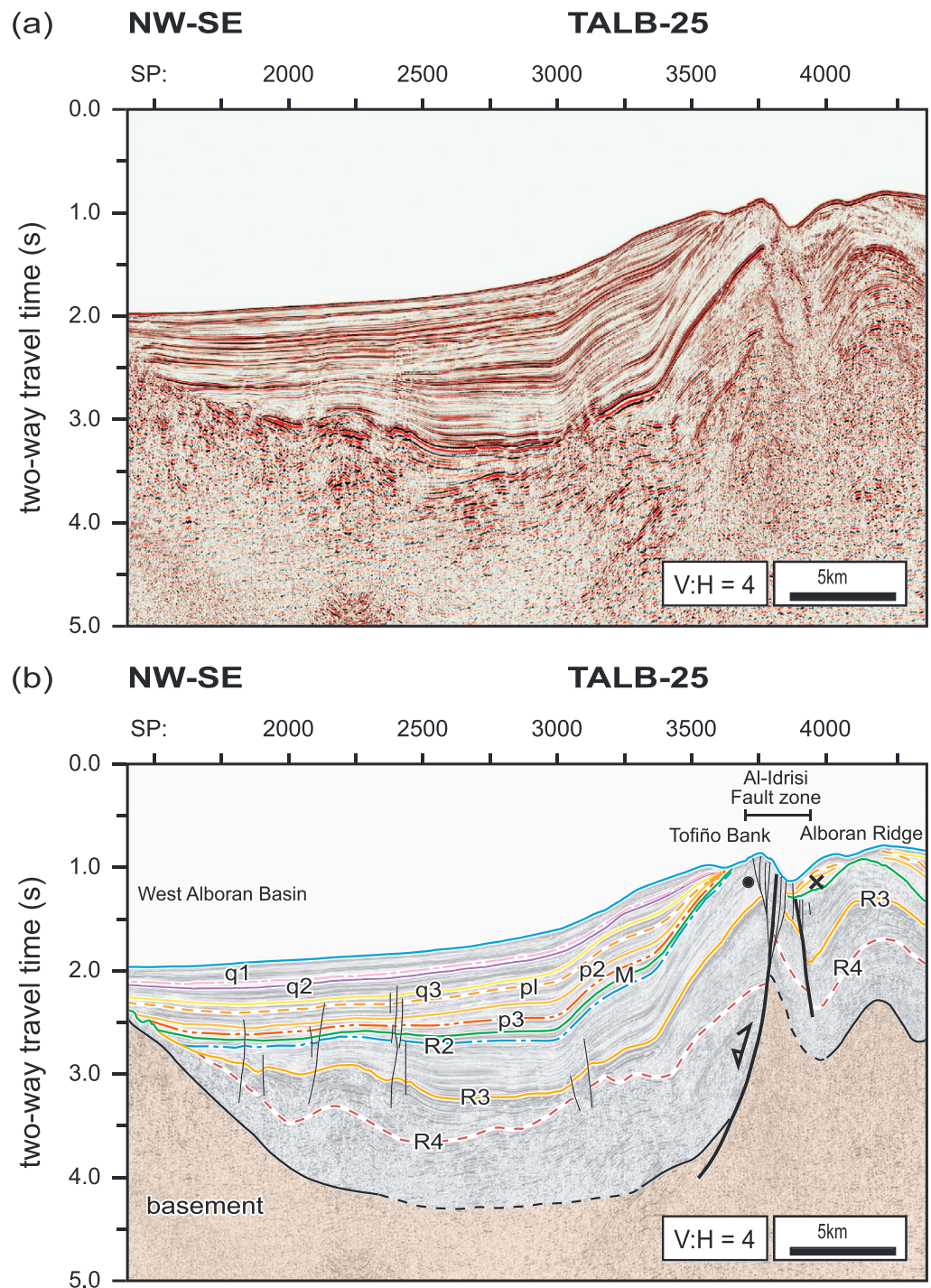


**Figure 5.** (a) Uninterpreted and (b) interpreted multichannel seismic section across the WAB, Al-Idrisi fault zone, Tofiño Bank, and Alboran Ridge. Key reflectors, age of unconformities, and seismic units as in Figure 4. The dashed lines indicate tentative position of top of basement. The location of seismic line is shown in Figures 3 and 6.

5.6–5.33 Ma (Clauzon et al., 1996; Krijgsman et al., 1999). However, it involves a much longer hiatus in other areas where it is strongly erosive.

The Miocene sequence in the study area was drilled at Habibas-1 well. ODP Sites 977 and 978 penetrated the Plio-Quaternary sequences and uppermost Messinian deposits, but not deeper. The Messinian sediments of Alboran (Unit II) are composed of marine and lacustrine sandy turbidites, fine-laminated sediments, and



shallow carbonates with occasional gypsum, anhydrite, and levels of volcanic ashes (Iaccarino & Bossio, 1999). The base of the unit is a late Tortonian R2 regional unconformity. Tortonian sediments mainly consist of sandstone intervals with claystone and silty-clay beds with turbiditic facies (Unit III). An angular unconformity at the base of this unit (R3) truncates the underlying sequences (e.g., Figures 4 and 5). The Serravallian to early Tortonian sediments (Unit IV) are graded sand-silt-clay turbidites and turbiditic muds, and their base is a strong reflector (R4). This surface forms an erosional truncation over large areas in the basin and changes laterally to a concordant surface in some deep parts of the basin (Figures 2, 4, and 5). At the Habibas-1 well the R4 reflector is a concordant surface within a sedimentary sequence of carbonate clays interbedded with sandy intervals of Serravallian age. In general, the Langhian to Serravallian deposits of Unit V include turbiditic sands and muds and undercompacted shales with sandy and pebbly intervals towards their base. The angular unconformity underlying these sediments (R5) has been interpreted as being formed during a major phase of extensional faulting (Comas et al., 1999). The lowermost deposits in the WAB are late Aquitanian (?) to Burdigalian and consist of mega-breccias and marine olistoliths embedded into overpressured fine-grained sediments forming Unit VI (Figure 2). The undercompacted shales of unit VI and from the base of unit V (subunit Vb) are the source layer for shale diapirs in the western Alboran Basin (e.g., Pérez-Belzuz, Alonso, & Ercilla, 1997; Soto et al., 2010).

#### 4.2. Basement

The top of acoustic basement corresponds to several discontinuous reflections of high amplitude and normal polarity forming a major unconformity at the base of the sedimentary cover (e.g., Figure 4). The underlying seismic unit with chaotic and semitransparent facies with low coherence is considered the true basement. In areas with a thin sedimentary infill the top of basement is clearly visible as a strong reflector with good lateral continuity. However, this reflector is more difficult to recognise when it lies under sediments thicker than 1 s twtt, due to the decreasing resolution of seismic profiles at greater depths. In such cases, the top of basement has been inferred. Locally, the top of basement can coincide with erosional palaeo-relief or fault surfaces bounding basement highs and tilted blocks and in places it consists of Miocene volcanic rocks (e.g., Figure 4).

Wells in the central Alboran Sea did not penetrate basement. However, the Habibas-1 well reached schist underlying the sedimentary cover at a depth of 4,496.5 m (Kheidri et al., 2000; Medaouri et al., 2014). Similar lithologies were drilled at DSDP Site 121 and ODP Site 976 on fault block highs in the WAB and along the northern margin of the basin in Alboran A-1 and Andalucía A-1 wells (Figure 1) (e.g., Jurado & Comas, 1992; Ryan et al., 1973; Soto & Platt, 1999). From these data it can be inferred that the Alboran Sea is underlain by continental crust. This is in agreement with basin-scale gravity and magnetic data (e.g., Galdeano et al., 1974; Watts et al., 1993).

### 5. Isopach Maps

Figure 6 shows the thicknesses of the Miocene and Plio-Quaternary sequences. For each map, faults thought to be active at each time interval are also shown. As discussed previously due to both imaging issue in the deep parts of the basin and the lack of stratigraphic data, the Miocene thickness map (Figure 6a) should be interpreted as a minimum illustrating the regional trend. Further uncertainties in this map result from the fact that in some places, the acoustic basement probably includes old sediments that were intruded or overlain by late Miocene igneous rocks (~12 to 6 Ma) (Duggen et al., 2004; Hoernle et al., 1999, and references therein); and some sediments originally deposited during the Miocene were later removed by erosional events such as that at M reflector times.

The Miocene thickness map illustrates a number of major sedimentary depocentres bounded by faults or volcanic highs (Figure 6a). The main SW-NE trend is clearly visible along the SAB, where sediments reach a maximum thickness of 2 km. In the westernmost part of the EAB, next to the Djibouti High, the SW-NE trending depocentre is up to 1.5 km thick. The two main troughs drilled at ODP Sites 977 and 978 in the centre of the EAB also correspond to two SW-NE trending Miocene depocentres up to 2.5 km thick. On the southern margin, a small SW-NE trending depocentre is located west of Melilla with a maximum thickness of ~1.5 km. The Habibas Basin has a maximum thickness of 2.4 km of Miocene sediments and forms an extensive depocentre. The depocentres along the axis of the WAB and the Yusuf basin have a secondary NW-SE orientation in contrast to the main SW-NE trend.



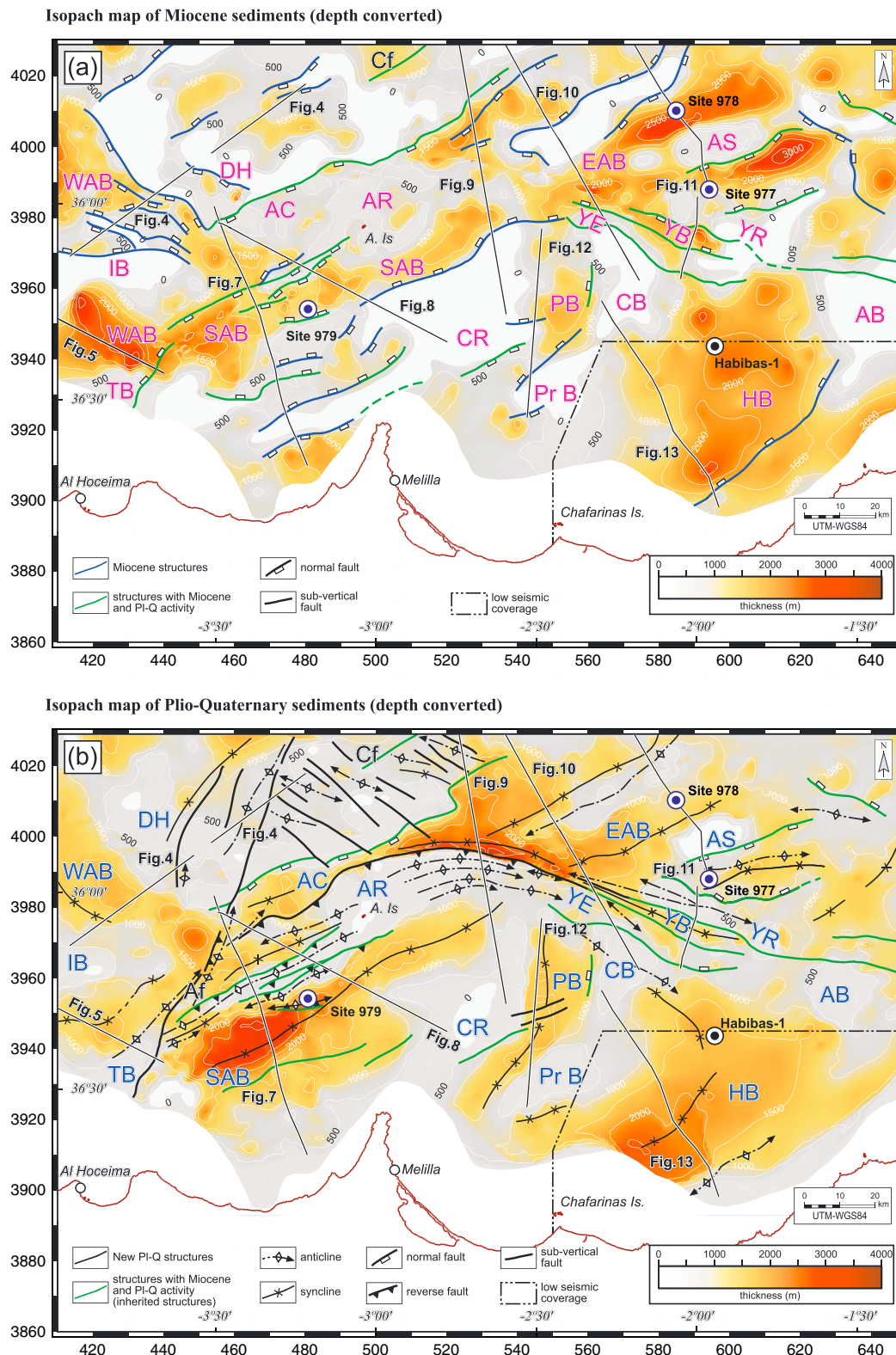


**Figure 6.** Isopach maps of (a) Miocene and (b) Plio-Quaternary sediments. Main structures active at each time interval are also represented. Contour interval is 500 m. UTM projection, units in kilometres. The black lines indicate multichannel seismic profiles presented in other figures. The circles are ODP sites 977, 978, 979, and the Habibas-1 well. Abbreviations: A. Is, Alboran Island; AB, Alidade Bank; AC, Alboran Channel; Af, Al-Idrisi fault; AR, Alboran Ridge; AS, Al-Mansour Seamount; CB, Câblers Bank; Cf, Carboneras Fault; CR, Cabo Tres Forcas Ridge; DH, Djibouti High; EAB, East Alboran Basin; HB, Habibas Basin; IB, Ibn-Batouta Bank; PB, Pytheas Basin; Pr B, Provençaux Bank; SAB, South Alboran Basin; TB, Tofiño Bank; YB, Yusuf Basin; YE, Yusuf Escarpment; YR, Yusuf Ridge; WAB, West Alboran Basin.

The Plio-Quaternary thickness map shows that some of the Plio-Quaternary depocentres are co-located with the main earlier Miocene depocentres along the SAB, EAB, Pytheas, and Habibas basins (Figure 6b). The Plio-Quaternary depocentre of the Alboran Channel trends SW-NE and merges with another NW-SE perpendicular subbasin in the WAB, thus following the older Miocene trends. The Plio-Quaternary filling of the EAB also has a complex geometry with several SW-NE to WSW-ENE elongated basin axes penetrated at ODP Sites 977 and 978 and contain up to 1 km of post-Messinian sediments. The two westernmost of these Plio-Quaternary depocentres thicken and deepen towards the SW, where they merge with a curved depocentre in front of the Alboran Ridge and Yusuf Escarpment. This arcuate depocentre, whose trend changes from SW-NE to NW-SE, is asymmetric and contains maximum Plio-Quaternary thickness up to 3 km. Other local maxima of Plio-Quaternary sediments are found in the Habibas Basin and SW of the SAB, respectively.

Comparing both maps, there are some important changes in basin depocentres through time. Both the SAB and Habibas Basins evolve to an asymmetric sediment distribution in the Plio-Quaternary, suggesting a post-Messinian tilting of these basins. Additionally, the locus of maximum sediment accumulation in the EAB moved from the east during the Miocene to a curved depocentre in front of the Alboran Ridge and Yusuf Escarpment, during the Plio-Quaternary. Some Miocene depocentres were no longer important sites of sediment accumulation during the Plio-Quaternary (Figure 6b).

## 6. Structures and Deformation

### 6.1. Miocene Structures

Most of the Miocene subbasins are bounded by SW-NE striking normal faults, except for those related to the NW-SE trending WAB and Yusuf Basin (Figure 6a). Seismic profiles show that many of these faults underwent an overprint of inversion, but in this section, we first focus on the extensional deformation. All the Miocene faults bound tilted blocks of basement, and most of the syn-rift deposits are sealed by the M reflector and covered by a thick sequence of Plio-Quaternary sediments (Figures 7–9). On many seismic profiles, strata can be seen expanding towards the footwall of the faults forming classic syn-rift growth wedges, indicating that the basins formed due to Miocene-aged rifting (Figures 4, 7, 10, and 11).

In the EAB, a system of Miocene normal fault-oriented SW-NE shows evidence of growth faulting until the Serravallian-Tortonian (Figures 6a, 9 (short point, SP 2,000–3,500), 10, and 11). Tilted strata of middle Miocene age occur in the hanging walls of the faults and are truncated by the R4 reflector. The R3 reflector seals most of these extensional structures in the EAB. Similar geometries have been observed along the Yusuf, Pytheas, and Habibas Basins (Figures 6a, 10–12, and 13). For example, in the Yusuf Basin, WNW-ESE trending, high-angle, normal faults bound a thick Miocene depocentre up to 1.3 s (twtt) (Figure 11). The fault at ~SP 1250 shows a significant normal slip component, and the entire Miocene sequence thickens towards the NE indicating growth faulting.

### 6.2. Plio-Quaternary Structures

All the structures active in Plio-Quaternary times show evidence for reverse or strike-slip movement (Figures 7–11). These include asymmetric folds, reverse faulting producing significant vertical displacements of all the key reflectors, and important thickness differences between fault blocks as seen along the northern margin of the Alboran Ridge. Strike-slip structures are imaged as subvertical overlapping fault segments with both reverse and normal displacements that cut the entire sedimentary cover and deform the seafloor indicating recent activity (Figures 4, 7, 8, 10, and 11). The main fault and fold systems active in Plio-Quaternary times coincide in location with earlier zones of Miocene deformation and display the same two structural trends: SW-NE and NW-SE. However, the SSW-NNE Al-Idrisi fault marks a new fault trend that cuts obliquely the westernmost sector of the Alboran Ridge (Figure 6b).

The northern flank of the Alboran Ridge is a south-dipping reverse fault with an arcuate trace in plan view and listric geometry in section (Figure 9). This fault zone curves to WNW-ESE orientation and links with the structures in the Yusuf fault zone to the east (Figure 6b). Uplift along the Alboran Ridge is documented by thinning of post M-reflector seismic units towards the anticline culmination and several angular unconformities (Figures 7, 8, and 9). The pl reflector marks a change of seismic facies from predominantly transparent Pliocene layers to mostly high-amplitude Quaternary units, and it reflects a change to more coarse-grained lithologies as a consequence of uplift and relief generation since ~2.45 Ma (e.g., Figures 7 and 12).

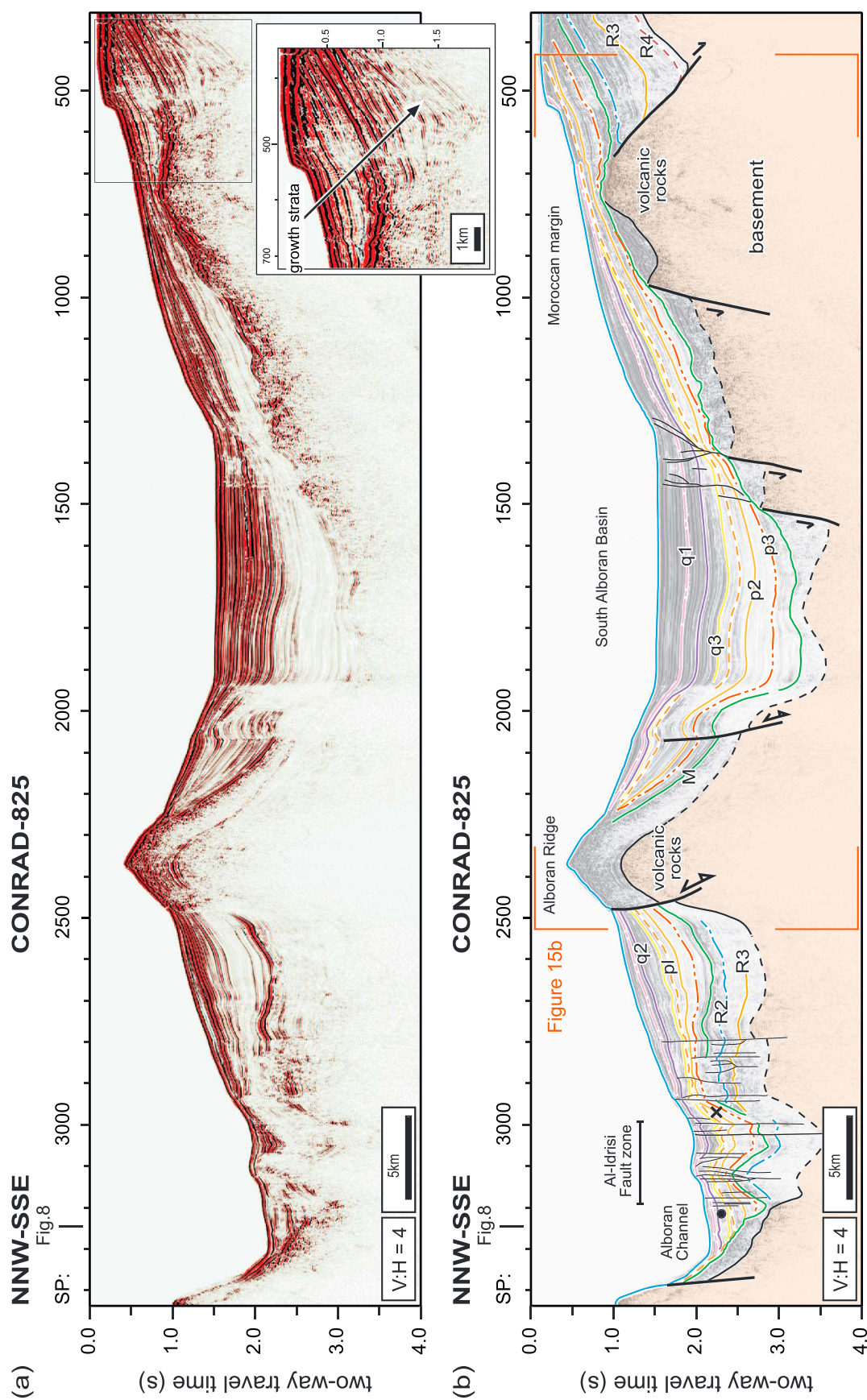


**Figure 7.** (a) Uninterpreted and (b) interpreted multichannel seismic section from the Alboran Channel to the North African Margin. Key reflectors, age of unconformities, and seismic units as in Figure 4. The dashed lines indicate tentative position of top of basement. The double arrows indicate Miocene normal faults inverted as reverse during the Plio-Quaternary. Location of seismic line is shown in Figures 3 and 6.



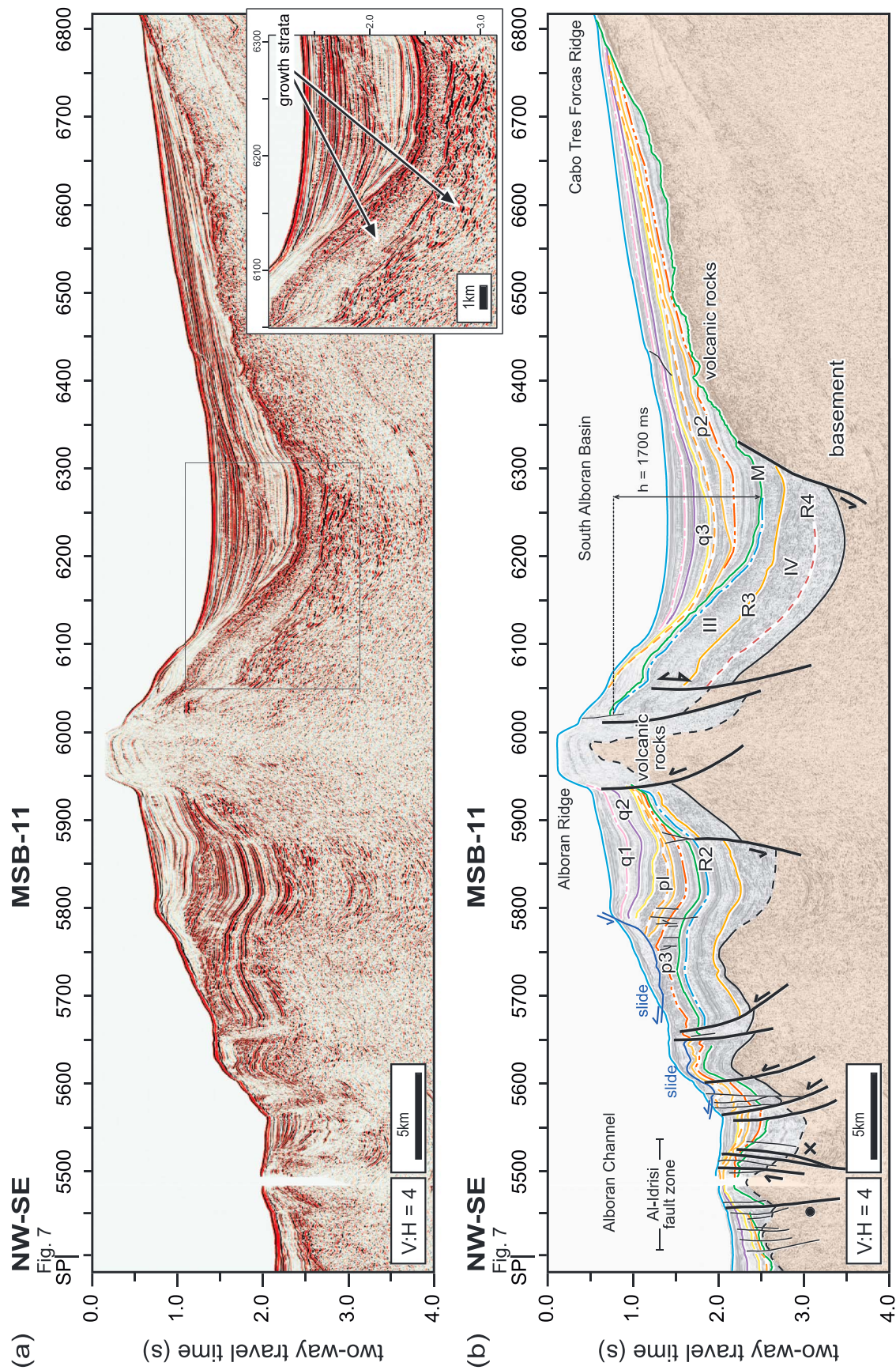


**Figure 8.** (a) Uninterpreted and (b) interpreted multichannel seismic section across the Alboran Channel, central Alboran Ridge, and SAB. Key reflectors, age of unconformities, and seismic units as in Figure 4. The dashed lines indicate tentative position of top of basement. The double arrow indicates a Miocene normal fault inverted as reverse during the Plio-Quaternary. Note the two growth wedges in Miocene sediments on the southern side of the Alboran Ridge and the SAB that thicken in opposite senses (SP 6,050–6,300): Unit IV (i.e., below R3 reflector) thickens towards the SE, while unit III (i.e., between R3 and R2 reflectors) thickens towards the NW. Location of seismic line is shown in Figures 3 and 6.



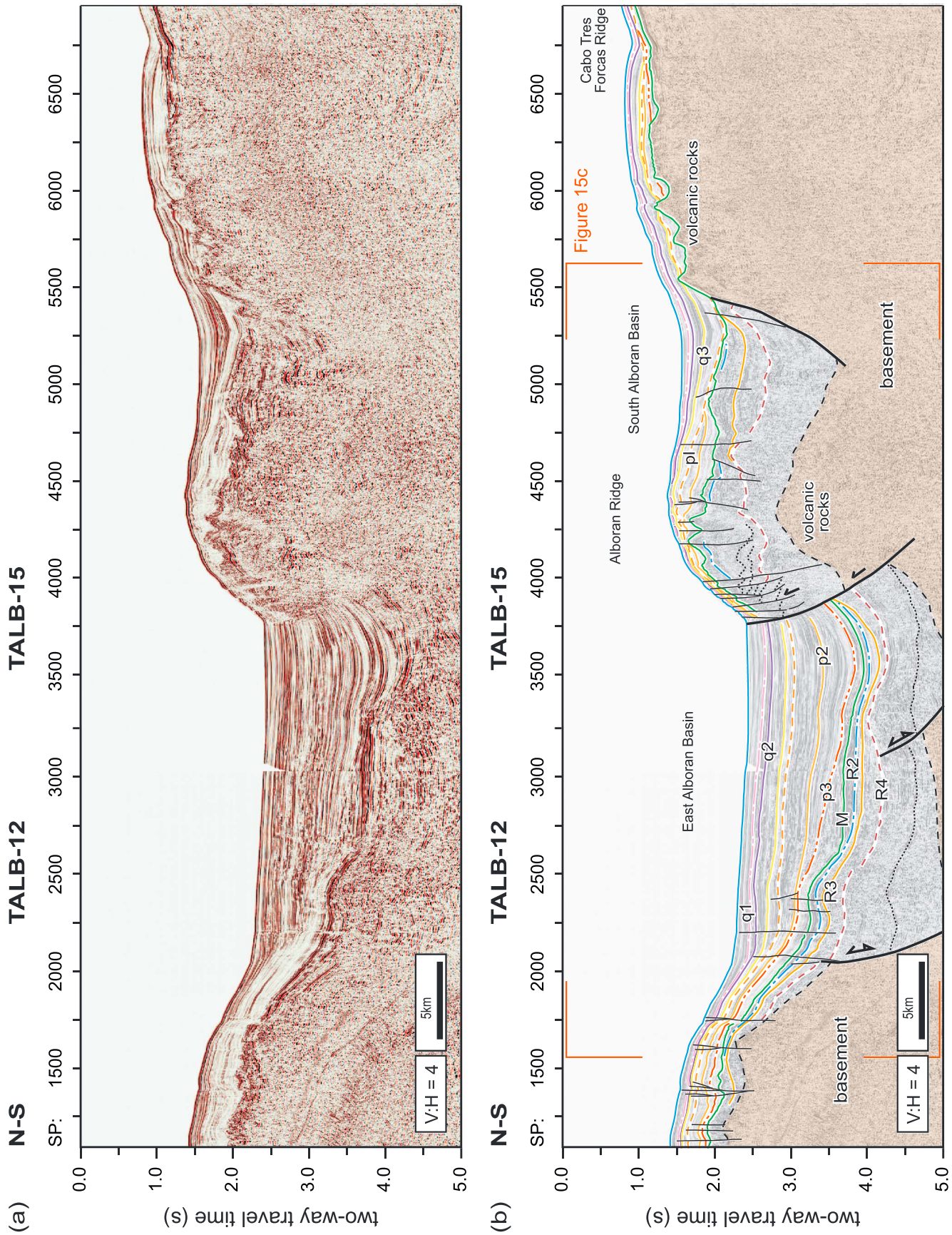


**Figure 9.** (a) Uninterpreted and (b) interpreted multichannel seismic section across the EAB, eastern Alboran Ridge, and SAB. Key reflectors, age of unconformities, and seismic units as in Figure 4. Note that the north-directed thrusting along the northern Alboran Ridge produced uplift of the Miocene depocentres on its hanging wall block causing basin inversion along the ridge itself and the SAB during the Plio-Quaternary. The dashed lines indicate tentative position of top of basement. The location of seismic line is in Figures 3 and 6.



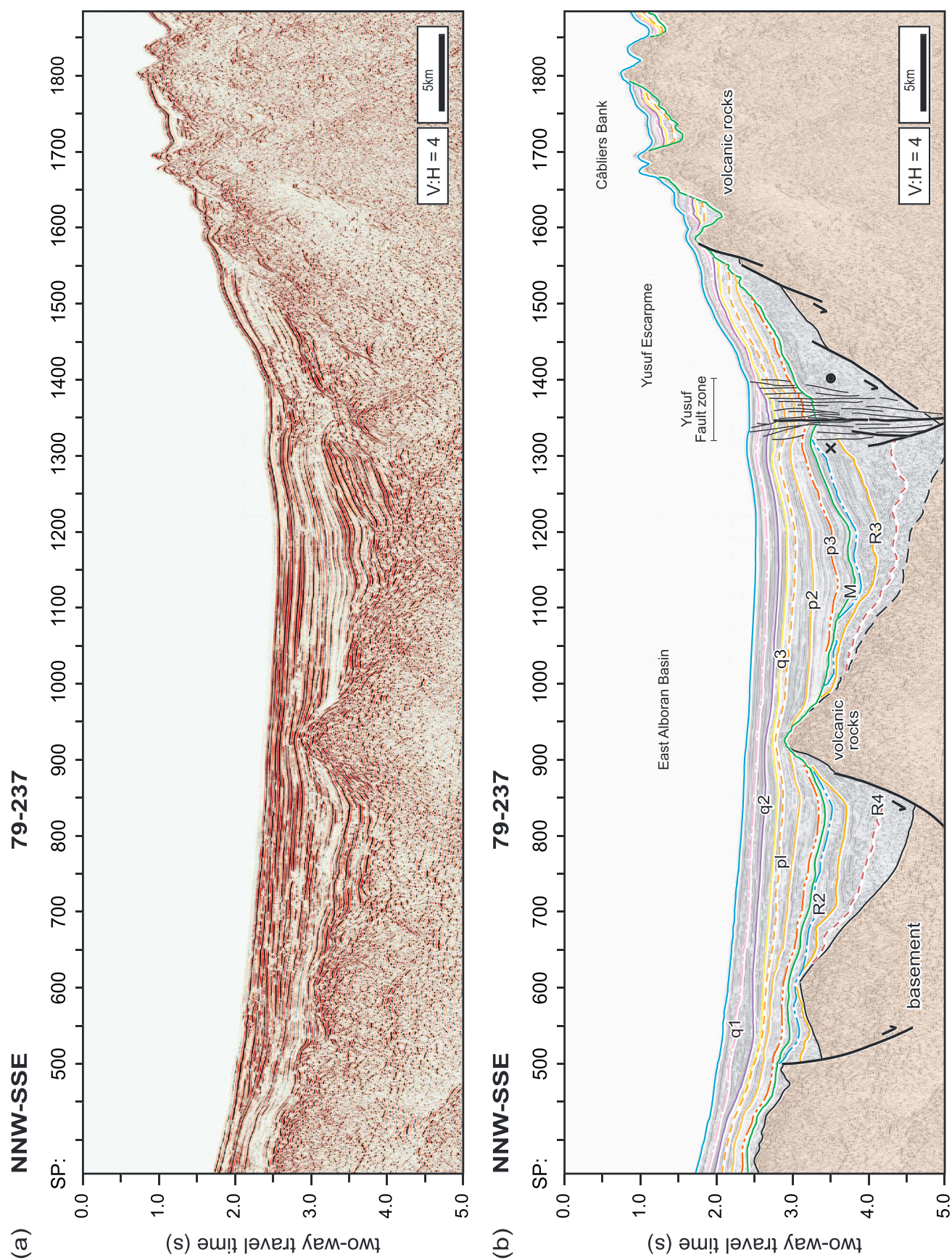


**Figure 10.** (a) Uninterpreted and (b) interpreted multichannel seismic section across the EAB and Yusuf Escarpment. Key reflectors, age of unconformities, and seismic units as in Figure 4. Note pre-M extensional structures and tilted blocks sealed by Plio-Quaternary sediments. The dashed lines indicate tentative position of top of basement. The location of seismic line is shown in Figures 3 and 6.



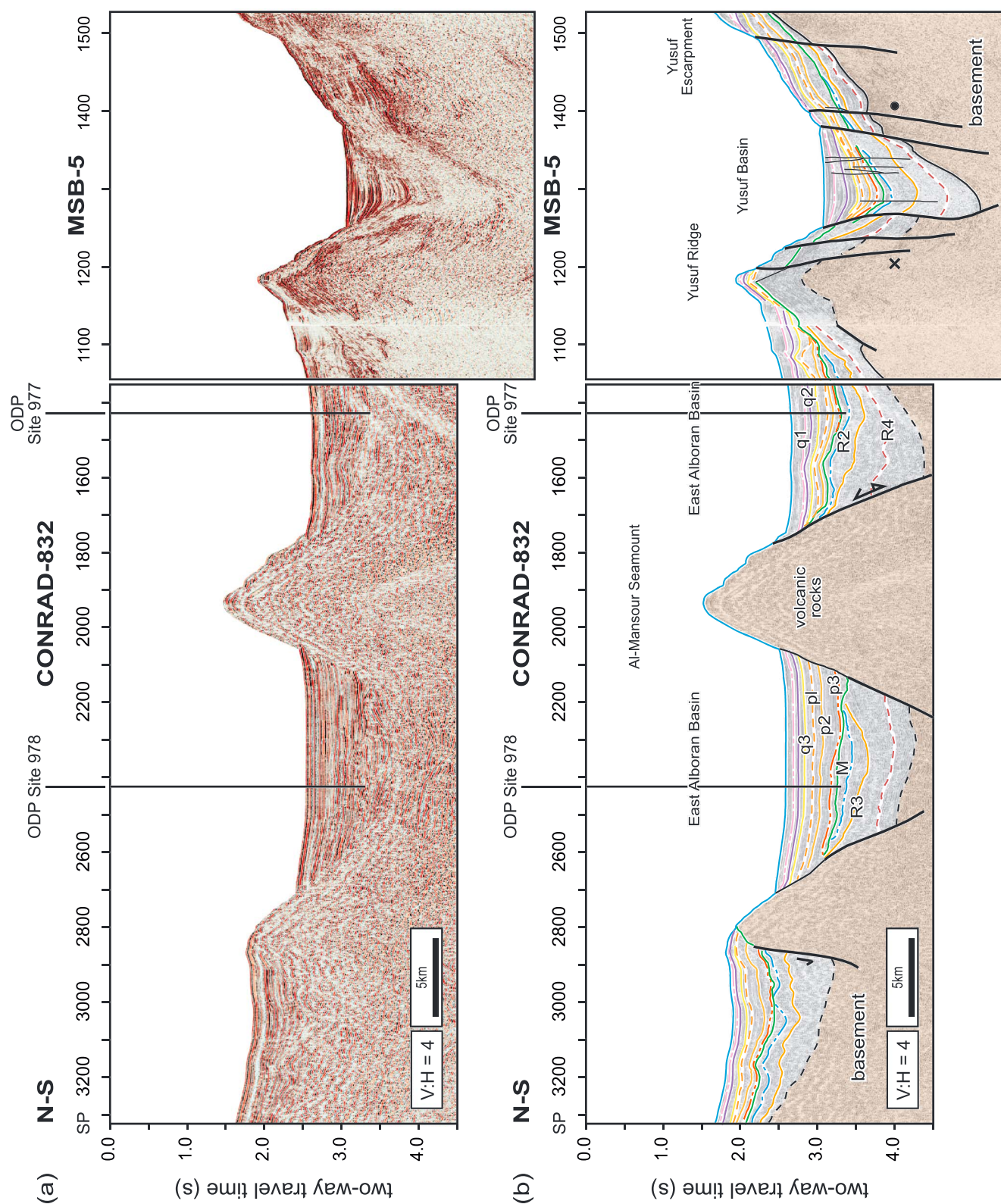


**Figure 11.** (a) Uninterpreted and (b) interpreted multichannel composite seismic section across the EAB and Yusuf Basin and ridge. Key reflectors, age of unconformities, and seismic units as in Figure 4. Note two small subbasins separated by a basement high in the EAB and perched sedimentary sequences on the margins of the Yusuf Basin. The dashed lines indicate tentative position of top of basement. The location of seismic line is shown in Figures 3 and 6.



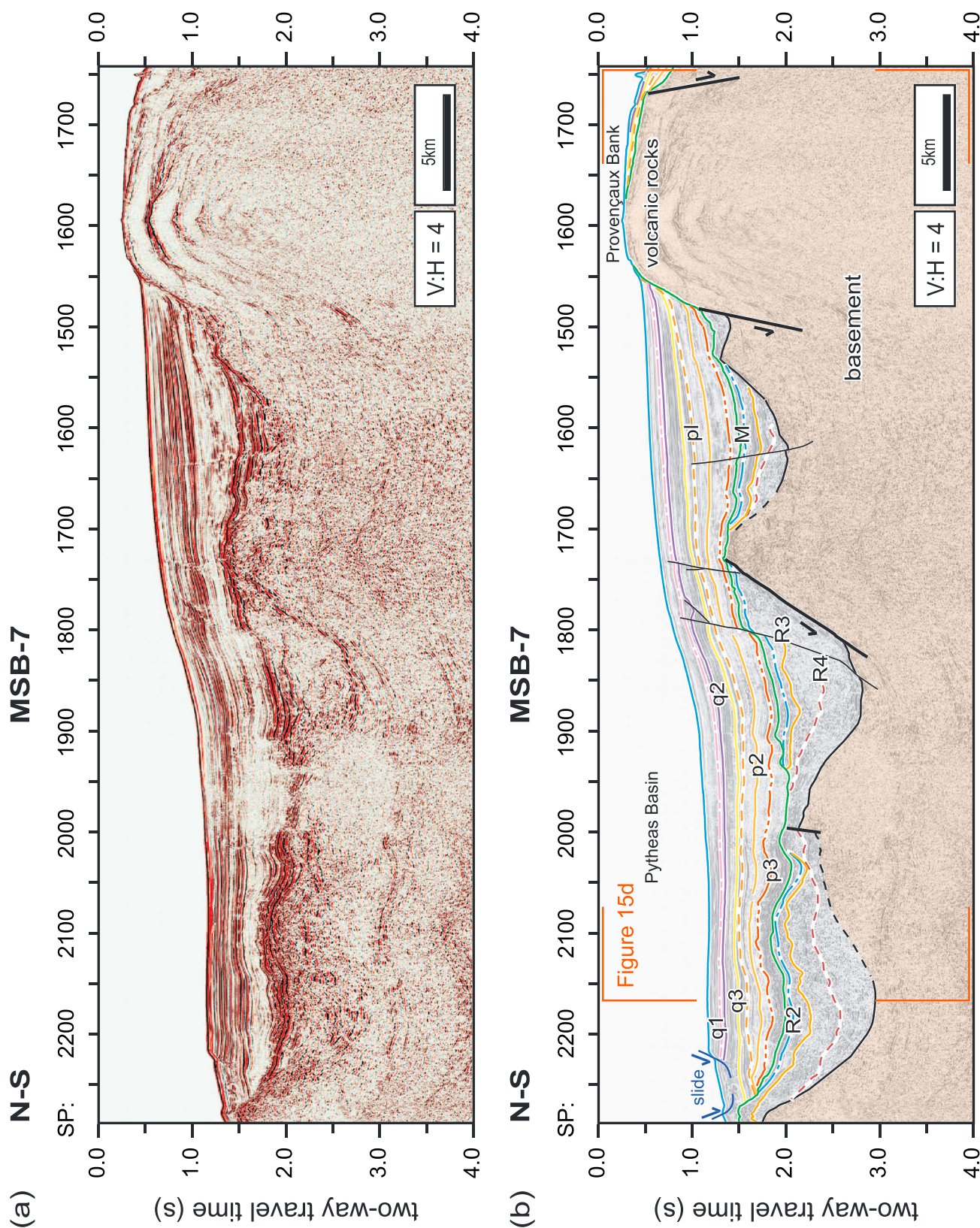


**Figure 12.** (a) Uninterpreted and (b) interpreted multichannel seismic section across the Pytheas Basin and Provençaux Bank. Key reflectors, age of unconformities, and seismic units as in Figure 4. The dashed lines indicate tentative position of top of basement. Note that Plio-Quaternary deposits seal most of pre-M extensional structures. The location of seismic line is shown in Figures 3 and 6.



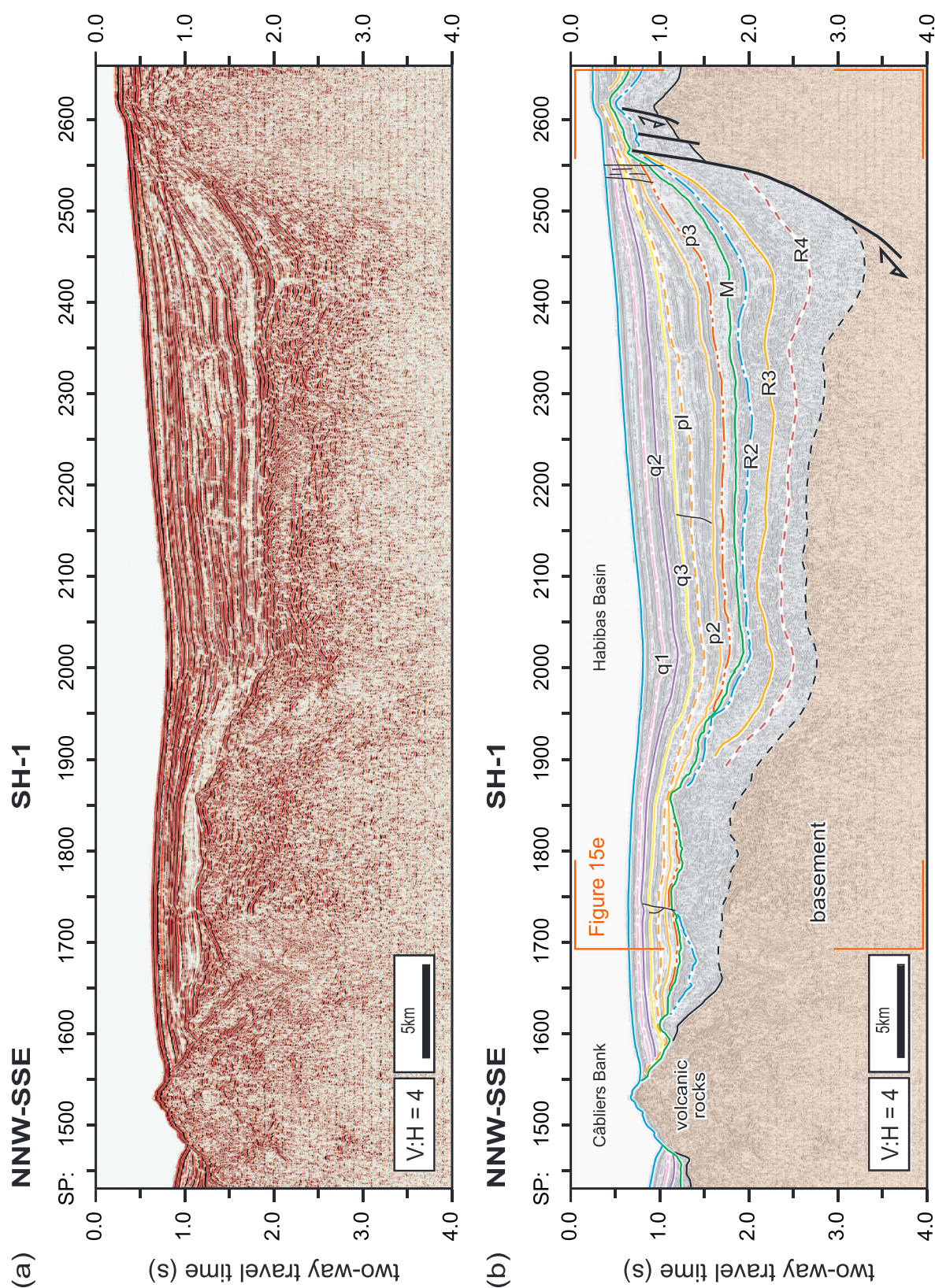


**Figure 13.** (a) Uninterpreted and (b) interpreted multichannel seismic section across the Habibas Basin. Key reflectors, age of unconformities, and seismic units as in Figure 4. Note growth wedge geometry for the lowermost deposits. The double arrows indicate inverted faults. The dashed lines indicate tentative position of top of basement. The location of seismic line is shown in Figures 3 and 6.

In the Yusuf Escarpment, post-Messinian deformation is concentrated along a narrow fault zone, ~4 km wide, with many subvertical faults and small normal slip components (Figure 10). Towards the east, the Yusuf fault zone becomes wider and comprises several faults with larger normal slip components, which bound the elongated and folded Plio-Quaternary depocentre of the Yusuf Basin (Figure 11). It should be noted that in the eastern sector of the Yusuf fault zone, the Miocene faults are reactivated, in contrast to the western sector where new faults were generated during the Plio-Quaternary (cf. Figures 10 and 11).

In many cases, the hanging wall blocks of Plio-Quaternary reverse faults contain folded and uplifted Miocene growth wedges indicating abundant post-Miocene reactivation and inversion (Figures 5, 7–9, and 13). The southern part of the Al-Idrisi fault zone is an example of an inverted structure that still remains in net extension (Figure 5). The strata between R5 and R3 reflectors can be seen expanding towards the SE in the hanging wall block of a Miocene normal fault (SP 2,750–3,750). Nevertheless, the whole sedimentary sequence is folded and uplifted in the Tofiño Bank and all the post-R2 seismic units thin towards the Alboran Ridge. These observations indicate that progressive, syn-sedimentary uplift occurred in this area at least since the Messinian.

Some other examples can be found along the Alboran Ridge, where we have mapped several asymmetric wedges of Miocene sediments that indicate the location of early syn-Miocene extensional activity on these faults. For example, Figure 7 shows that the core of the western Alboran Ridge comprises a fold involving Miocene sediments (shot points (SP) 2,100 to 2,500). At present day, these deposits form the hanging wall of a Plio-Quaternary reverse fault, but they thicken towards the NW. These observations suggest that the SE-dipping fault was originally an extensional fault in the Miocene forming a half-graben filled by sediments that were later inverted. Similarly, there are other growth wedges in the southern slope of the Alboran Ridge (Figure 8, SP 6,025 to 6,300). In this case the R3 and M reflectors bound a sedimentary sequence thickening towards the NW that suggests the existence of an SE-dipping extensional fault active in late Miocene times. Inversion and uplift are demonstrated by the fact that the syn-growth wedge is folded and covered by a thick Plio-Quaternary sequence of about 1,200 ms (twtt) in the SAB that progressively thins to ~200–400 ms (twtt) in the slope of the Alboran Ridge, where the sequence is uplifted about 1,700 ms (twtt) compared to the wedge apex in the centre of the SAB.

The SE margin of the Habibas Basin is formed by a Miocene half-graben with a northwest-facing border fault (Figures 6a and 13). The basin is filled with a syn-rift Miocene sequence, penetrated at Habibas-1 well, which expands towards the footwall scarp and reaches a maximum thickness up to 1.7 s (twtt). The growth wedge is uplifted close to the normal fault, and all the sediments below the p2 reflector are folded.

## 7. Timing and Distribution of Tectonic Inversion

The spatial and temporal distribution of deformations is summarized in Figure 14. The main areas of Plio-Quaternary uplift (stippled pattern) are superimposed on the distribution of Miocene depocentres and structural interpretations in Figure 14a. Areas undergoing uplift are defined as those where any of the p2 to q1 surfaces form strong erosional angular unconformities documenting the main Plio-Quaternary tectonic events (Martínez-García et al., 2013). Thus, the portions of Miocene depocentres matching the shaded stippled pattern represent those parts of the extension-related basins that were uplifting in late Pliocene to Quaternary times. Inversion is mainly focused along two SW-NE trending domains: (1) the western Alboran Ridge and locally affecting some nearby sectors of the SAB and WAB and (2) the southeastern part of the Habibas Basin. Other small portions of uplifted Miocene depocentres occur along the Yusuf fault zone and small folds in the EAB.

Spatial and temporal constraints based on the geometry of sedimentary units and the position of key reflectors along the different fault blocks of inverted faults indicate that the studied structures have different magnitudes of tectonic inversion. Tectonic inversion was partial along the central Alboran Ridge and Habibas Basin (Figures 8, SP 6,025–6,300 and 13, SP 1,900–2,550). In both cases, the uplifted hanging walls, which contain deformed syn-rift sequences, still remain in net extension with respect to the footwalls, and none of the syn-rift markers have reached their null points revealing that shortening did not compensate the bigger amount of previous Miocene extension. Thinning of postrift units mainly occurs next to the reactivated fault planes. Conversely, in the western Alboran Ridge, tectonic inversion was complete (Figure 7). The syn-rift sequence, originally deposited along a Miocene half-graben, has been totally inverted and folded, becoming an uplifting high with little to no Plio-Quaternary sediments on top.



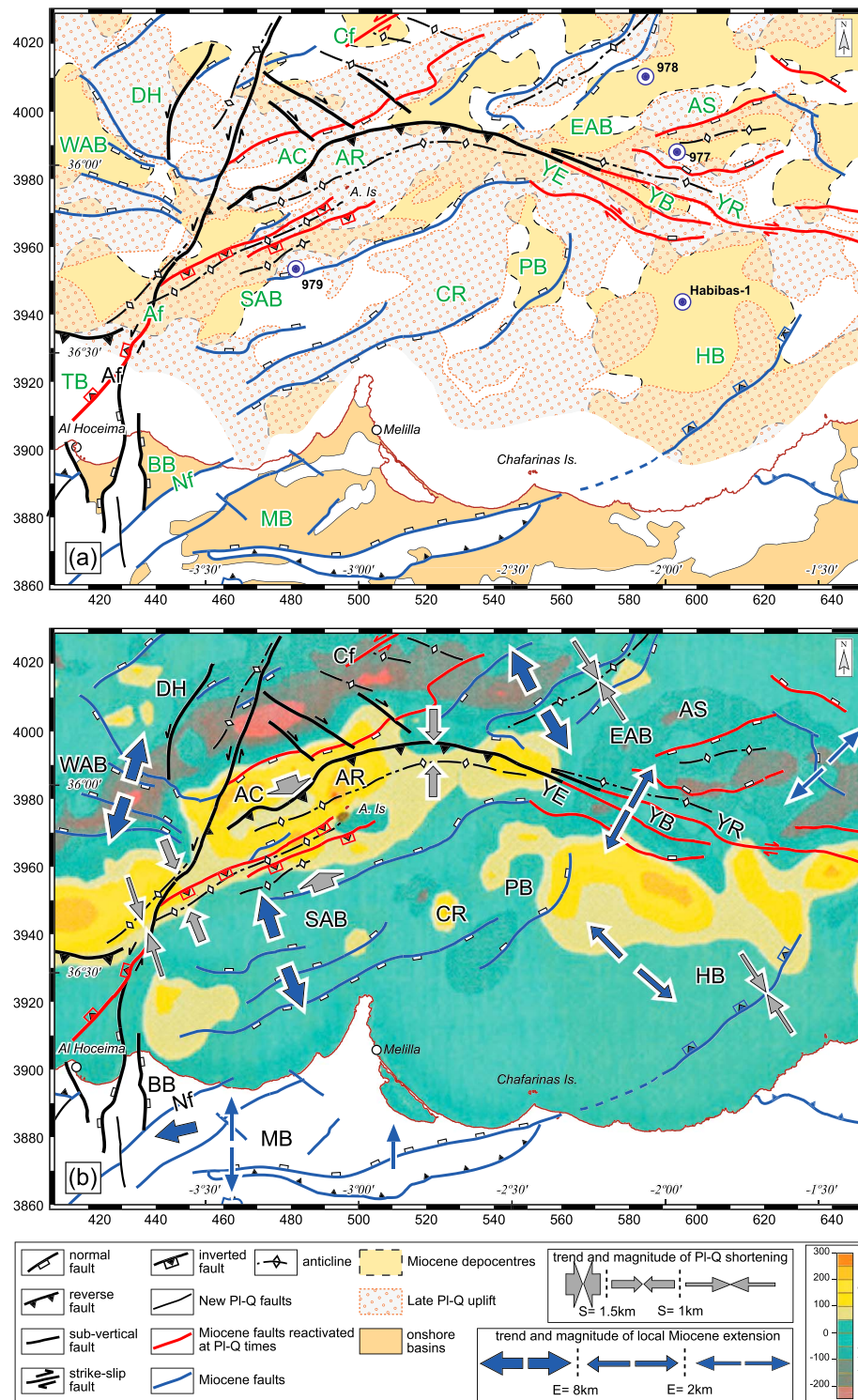


**Figure 14.** (a) Map comparing the distribution of Miocene depocentres (Figure 6a) with the main Plio-Quaternary uplifting realms, where the p2 to q1 surfaces are significant erosional angular unconformities (Martínez-García et al., 2013). Note uplifted Miocene depocentres related to inverted faults along the Tofiño Bank, Alboran Ridge, SAB, and Habibas Basin. (b) Magnetic anomalies and tectonic map. (c) The blue and grey arrows indicate minimum magnitudes of Miocene extension (E) and late Pliocene to Holocene shortening (S), which were estimated for the top of basement and p2 reflectors (~3.28 Ma), respectively, using line-length restoration analysis from depth-converted interpretations of seismic profiles. Estimations in North Morocco come from Azdimousa et al. (2007). The map of magnetic anomalies is taken from Willet (1997). Abbreviations: A. Is, Alboran Island; AC, Alboran Channel; Af, Al-Idrisi fault; AR, Alboran Ridge; AS, Al-Mansour Seamount; BB, Boudinar Basin; Cf, Carboneras Fault; CR, Cabo Tres Forcas Ridge; DH, Djibouti High; EAB, East Alboran Basin; HB, Habibas Basin; MB, Melilla Basin; PB, Pytheas Basin; SAB, South Alboran Basin; TB, Tofiño Bank; YB, Yusuf Basin; YE, Yusuf Escarpment; YR, Yusuf Ridge; WAB, West Alboran Basin.

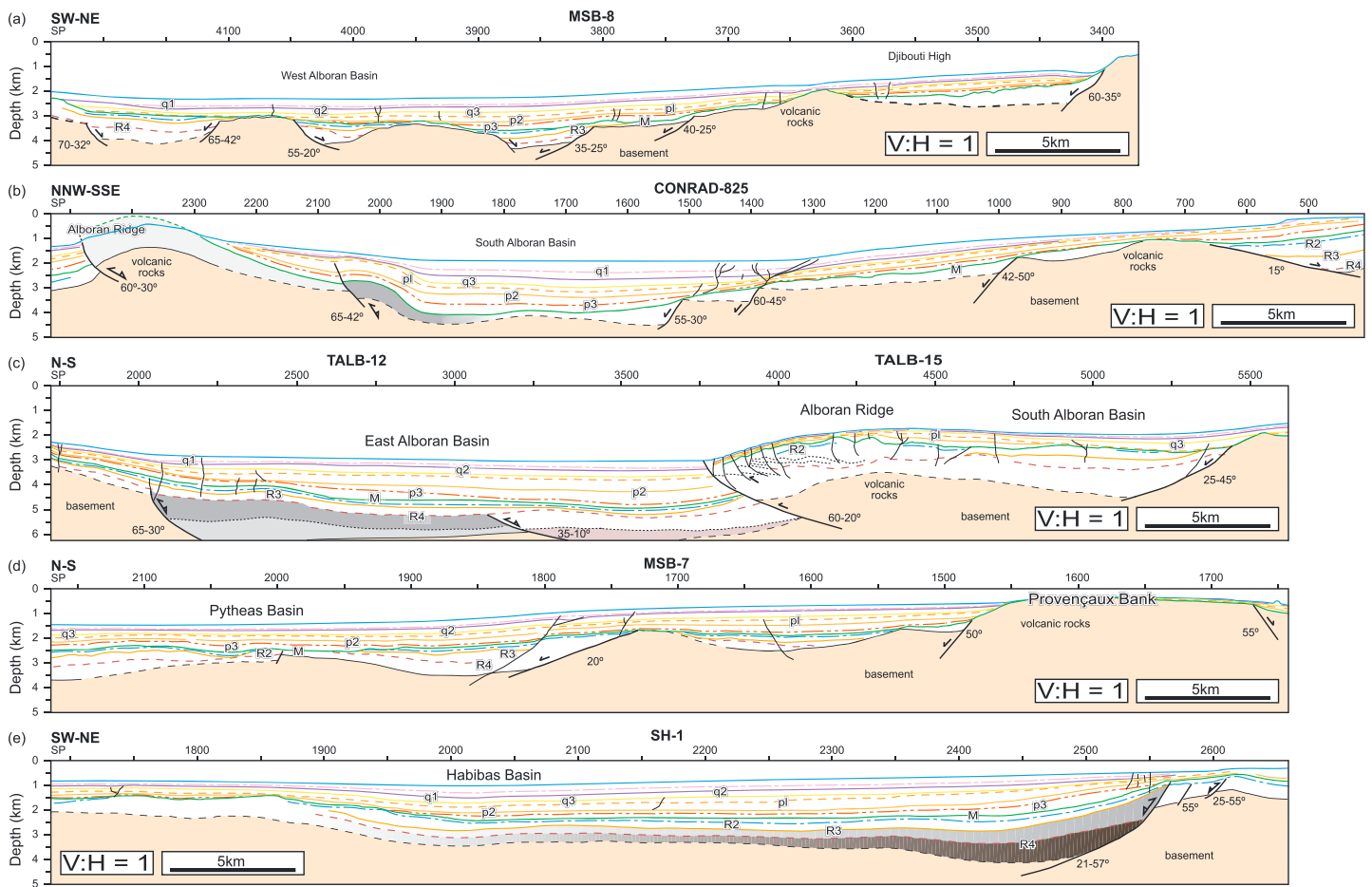


**Figure 15.** Depth-converted interpretations of selected segments of seismic profiles presented in other figures, which were obtained using the interval sonic velocities ( $V_p$ ) shown in Figure 2. Depths in metres below sea level. The major, inverted, syn-rift growth wedges are shown in grey. The location of profiles is shown in Figure 3.

The timing of inversion is also variable. The Habibas half-graben began to shorten in late Tortonian times as seismic units on top of the R3 reflector do not show any more growth-strata towards the footwall scarp. Instead, post-R3 units thin towards the fault revealing its reverse reactivation (Figure 13). The M reflector seals the fault zone, indicating that it became inactive before the Plio-Quaternary. However, the gentle anticline deforming the sediments between the R3 and p2 reflectors at ~SP 2,500–2,700 might indicate a further continued reactivation and uplift caused by early Pliocene shortening along the Habibas Basin. In the EAB, SW-NE trending anticlines linked to underlying Miocene normal faults also suggest contractional fault reactivation, but starting at post-R4 times and ending at p2 reflector times (Tortonian to late Pliocene) (Figure 9, SP 2,400 and 3,300). In contrast, in the southern Al-Idrisi fault and central Alboran Ridge, the switch from thickening pre-R2 Miocene sediments towards the fault to thinning of the most recent overlaying units into the Alboran Ridge anticline suggests that inversion started in the latest Tortonian and continued to the present day (Figure 5, SP 1,500–3,750; Figure 8, SP 6,025–6,300). In the western ridge, the main uplift due to inversion and folding has occurred since the early Pliocene as revealed by the p3 to q1 unconformities and expansion of sedimentary sequence away from the Alboran Ridge (Figure 7).

## 8. Extension and Shortening Strain Estimations

We used depth-converted interpretations to estimate the amount of extension and shortening (Figure 15). The depth-converted data show that in general, Miocene normal faults have variable dips and they are often listric in geometry. High-angle normal faults (~45°–65°) are mainly located along the margins of the main SW-



NE trending basin (e.g., SP 2,100 in Figure 15c; SP 1,525 in Figure 15d; SP 2,560 in Figure 15e). Within synthetic systems of normal faults, the dips progressively decrease towards the basin centres, and faults in the inner parts of the basin are typically lower angle. (e.g., Figure 15c, SP 2,000–3,525). The inverted Miocene structures along the Alboran Ridge and Habibas Basin are listric faults. Their dips range from  $\sim 60^\circ$  on the shallower parts to  $20^\circ$ – $30^\circ$  in depth (Figure 15b, SP 2,500–2,400; Figure 15e, SP 2,450–2,560).

The amount of Miocene extension ( $E$ ) was determined for the top of basement and compared to the later shortening ( $S$ ) (Figure 14b). The distribution of magnetic anomalies revealing the location of main volcanic intrusions is also shown. The uncertainties in the position of the top of basement for the deepest basins were taken into account considering the maximum and minimum possible basement depths in each section. Magnetic data also helped to better constrain the geometry of the top of the basement. The potential errors derived from this method limitation are always less than 5% of the obtained values of  $E$ . We estimated shortening ( $S$ ) values for the p2 reflector ( $\sim 3.28$  Ma; Figure 2) because the older post-Messinian unconformity, the p3 reflector, has a limited presence in the area (Martínez-García et al., 2013). Thus, the  $S$  values presented here are minimum and only represent late Pliocene to present-day shortening. It should be also noted that line-length restorations underestimate  $E$  and  $S$ , as they do not include (1) thickness variations during deformation; (2) subseismic-scale structures; (3) displacements due to oblique deformation and strike-slip components; and (4) the amounts of  $E$  that cannot be measured because of later inversion. The last factor is probably the most important for the measurement of inversion-related strain for the Alboran Sea, as most of shortening is accommodated by reverse fault displacement of former extensional faults that needed to have all their normal-sense displacement “restored” before they begin to accumulate net reverse offset. The values in Figure 14b are therefore only first order, minimum estimations.

Maximum amounts of extension are up to 17 km in the easternmost part of the WAB and trend SW-NE (Figure 14b). The axis of the extensional strain has a similar orientation in the Yusuf Basin and further to the east towards the Algerian Basin, but the magnitudes are considerably smaller (5–6 km). In both the southwestern SAB and the EAB, the amount of extension is up to 10 km and the inferred extension direction is NW-SE. The extension in the Pytheas and Habibas basins was WNW-ESE directed, but the calculated magnitudes are smaller (4–6 km). In comparison, the shortening directions are largely consistent across the area and mainly trend NW-SE, perpendicular to the strike of the Alboran Ridge and oblique to the Al-Idrisi fault zone. Maximum values, up to 2 km, are found at the central Alboran Ridge and decrease to 1–1.5 km towards its northeastern and southwestern ends. The estimated shortening for the Habibas Basin is less than 1 km.

## 9. Discussion

### 9.1. Miocene Rifting in the Alboran Sea Basin

Crustal stretching and rifting of the Alboran Domain started at about 27 Ma (late Oligocene) according to exhumation histories of metamorphic rocks from the basin basement (e.g., Platt et al., 1998). Rapid subsidence took place from the early Miocene to Langhian-Messinian and was followed by a slower thermal subsidence until the present day (e.g., Docherty & Banda, 1995; Hanne et al., 2003; Watts et al., 1993). Extension started while the region was elevated above sea level and denuded the thickened continental crust in the inner part of the Alpine collisional orogen. At  $\sim 23$ – $18$  Ma (Aquitanian?–Burdigalian), tectonic subsidence gave way to a marine transgression, as indicated by the presence of marine deposits encountered in the WAB where the Alboran Sea began to form (e.g., Chalouan et al., 1997; Iribarren, Vergés, & Fernández, 2009; Jurado & Comas, 1992; Pérez-Belzuz et al., 1997). Miocene tectonic subsidence was controlled by extensional systems of low-angle, normal faults, and ceased by late Tortonian ( $\sim 9$  Ma) (Bourgeois et al., 1992; García-Dueñas et al., 1992; Martínez-Martínez & Azañón, 1997). Onshore, in the central Betics, a Burdigalian to Langhian system produced NNW-SSE extension, and Serravallian to lower Tortonian faults controlled a later episode of NE-SW extension (Martínez-Martínez, Soto, & Balanyá, 2004, and references therein). In the Rif, Tortonian deposits seal normal fault systems that show extension with SSW-directed or NE-directed transport directions (e.g., Booth-Rea et al., 2012; Chalouan et al., 2008) (Figure 1). The Jebha and Nekor faults acted as left-lateral transfer faults accommodating variable rates of extension between the major normal-fault systems during the Oligocene to middle Miocene (e.g., Achalhi et al., 2016; Benmakhlouf et al., 2012; Galindo-Zaldívar et al., 2015). A later Miocene N-S extension controlled the formation of the southern Melilla Basin (e.g., Azdimousa et al., 2007). Offshore, extension had a top to the S to SE sense of movement along the

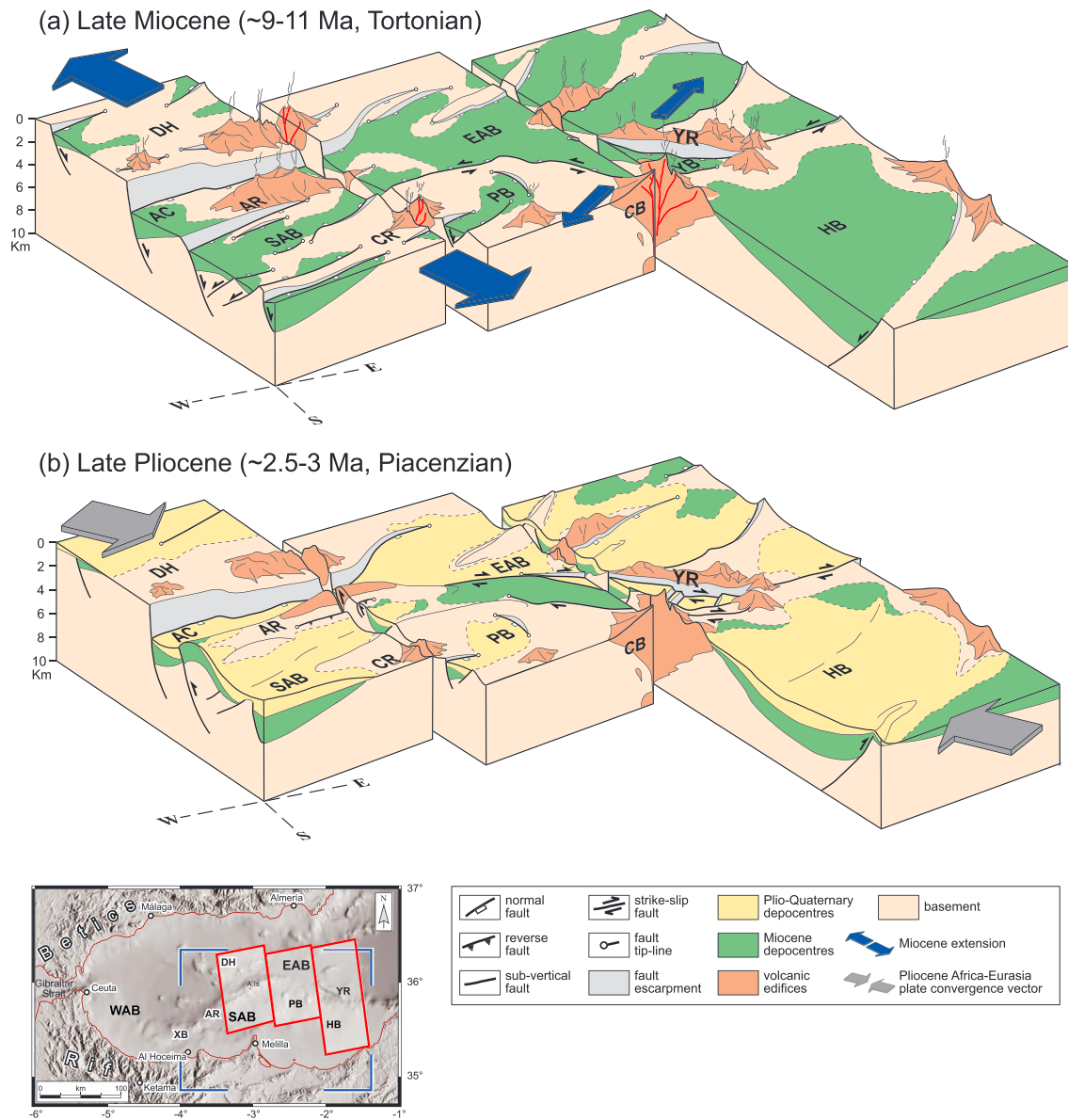


**Figure 16.** 3D sketches summarizing the tectonic inversion of the central and southeastern Alboran Sea. The evolution is analysed comparing two stages during the late Miocene and late Pliocene. Miocene deformation took place in context of west directed movement of the entire basin. Abbreviations: AC, Alboran Channel; AR, Alboran Ridge; CB, Câbliers Bank; CR, Cabo Tres Forcas Ridge; DH, Djibouti High; EAB, East Alboran Basin; HB, Habibas Basin; PB, Pytheas Basin; SAB, South Alboran Basin; YB, Yusuf Basin; YR, Yusuf Ridge.

northern Alboran margin changing to a dominantly NE transport direction in the WAB, but little is known about the extension trends in other sectors of the Alboran Sea (Ammar et al., 2007; Chalouan et al., 1997; Comas et al., 1999).

Figure 14 suggests a crustal extension of ~20%, which is insufficient to explain the generation of the accommodation space of the observed Miocene depocentres that reach up to 2.5 km (Figure 6a). Previous independent estimates of extension obtained from backstripping analyses of well data at the northern margin of the basin reveal much greater amounts of extension, with  $\beta$ -factors of 1.4 to 2, indicating that rapid lithospheric stretching thinned the crust below the Alboran Sea to 15–20 km (Docherty & Banda, 1995; Hanne et al., 2003; Watts et al., 1993). Flexural modelling suggests that the shallow emplacement of asthenosphere created a large thermal sag in the WAB overprinting the effects of rifting (Do Couto et al., 2016; Morley, 1993). This is in agreement with the onlapping distribution of Miocene sediments in the EAB, where each unit covers the lower one, leading to the expansion of the basin area (Figures 9 and 10).



Tortonian magmatic activity may also have masked the importance of the extension as volcanic rocks may have intruded along Miocene fault planes obscuring any imaging of greater displacements (Figure 16a). Calculation of extension using regional-scale seismic sections underestimates the true amount of extension because the contribution from smaller faults beneath seismic resolution is omitted. Nevertheless, the distribution and geometries of Miocene structures reported here for the less explored sectors of the Alboran Basin can shed light on the knowledge of the rifting episode at a regional scale. The predominant trend of Miocene extension in the central and southeastern Alboran is NW-SE (Figure 14b). Comparing the directions previously recognized for the WAB and the Betic and Rif margins (Figure 1) with this inferred NW-SE extension along the Alboran Ridge, SAB, and Habibas Basin, an extensional system with an overall radial pattern that seems to mimic the curved shape of the orogenic front can be reconstructed. It should also be noted that ~200 km of N-S convergence between the Eurasian and African plates was synchronous with the oblique SW-directed migration by ~250 km of the entire Alboran Domain during the Miocene (e.g., Andrieux et al., 1971; Dewey et al., 1988; Platt & Vissers, 1989; García-Dueñas et al., 1992; Rosenbaum et al., 2002). Considering this complex scenario, the Miocene SW-NE trending normal faults recognized in the central and southern Alboran Sea could have had a significant strike-slip left-lateral component and therefore may have acted as transtensional structures. This is consistent with the Miocene strike-slip movement of the SW-NE trending Jebha and Nekor faults reported onshore Morocco (e.g., Achalhi et al., 2016; Azdimousa et al., 2007; Benmakhlouf et al., 2012; Chalouan & Michard, 2004) and would also agree with the hypothesis that the Alboran Channel began to form as a Miocene transtensional corridor bounded by two SW-NE trending faults (Willet, 1997).

The WAB and northern Alboran margin contains up to 6 km of Miocene sediments, with the oldest deposits being ~23–18 Ma (Aquitian?–Burdigalian), with rifting ending between 9 and 7 Ma (Tortonian) (Comas et al., 1999). We deduced a similar age of end of rift-related extension in the central and southeastern Alboran Sea. However, the oldest deposits in the study area penetrated at Habibas-1 well are Serravallian and the preserved Miocene depocentres are 2.5–3.5 km thick in the EAB. Thus, Miocene sediments in the central and southeastern Alboran Sea are probably younger and thinner than those in the western and northern parts of the basin.

Onshore-offshore correlations indicate that the Boudinar and Melilla basins are the emergent parts of the SAB (Achalhi et al., 2016; Cornée et al., 2016) (Figure 1). The two main structural trends in the Moroccan basins can be correlated with the extensional episodes recognized in the Alboran Sea. SW-NE trending extensional detachments exhumed the metamorphic basement of the Boudinar and Melilla basins during the Tortonian indicating a top to the SW sense of movement (e.g., Azdimousa et al., 2007; Booth-Rea et al., 2012) (Figures 1 and 14). This extension was synchronous with the left-lateral movement of the Nekor Fault and resulted in the opening of continental basins at ~10.5 Ma (Chalouan et al., 2008; Cornée et al., 2016; Galindo-Zaldívar et al., 2015). In the Melilla Basin, the low-angle extensional detachments were cut by later WSW-ENE trending systems of high-angle normal faults recording a younger episode of N-S extension. Marine incursions from the Alboran Sea to the North African basins occurred from late Tortonian to Quaternary (Achalhi et al., 2016; Poujol et al., 2014). Thus, the offshore Miocene SW-NE trending depocentre to the NW of Melilla might be the continuation of the northern Melilla Basin (Azdimousa & Bourgois, 1993) (Figure 14).

The age and orientation of Miocene extensional systems in the central Alboran Sea also resemble their analogue structures to the east in Algeria (Figure 1). The SW-NE to WSW-ENE trending systems of normal faults in the Algerian margin subbasins are filled by syn-rift deposits and mostly sealed by Messinian sediments (e.g., Domzig et al., 2006; Mauffret, 2007; Rehault, Boillot, & Mauffret, 1984; Yelles et al., 2009). Crustal thinning along the Algerian margin was greater than the Alboran area and led to W-E to SW-NE directed sea-floor spreading at ~16–8 Ma and formation of oceanic crust (Galdeano, 1974; Catalano et al., 2000; Mauffret et al., 2004; Strzeczynski et al., 2010). The transition from the thin continental crust of the Alboran area to oceanic crust in the Algerian Basin is progressive and occurs along the EAB, where magmatic intrusions show a combination of tholeiitic and calc-alkaline signatures characteristic of immature oceanic or transitional crust (e.g., Duggen et al., 2004; Giaconia et al., 2015). In this setting, the Miocene normal faults along the Yusuf and Habibas escarpments played an important role forming a lithospheric boundary between the thinned continental crust of Alboran and the new oceanic basement of the Algerian Basin (Leprêtre et al., 2013; Medaouri et al., 2014). The Miocene Yusuf fault could have had a significant left-lateral strike-slip component, as its WNW-ESE trend was oblique to the SW-directed migration of the Alboran Domain (Figure 16a). Similar Miocene kinematics has been inferred for the Habibas Escarpment, marking the steep margin transition from the Tell continental domain to the Algerian Basin (Medaouri et al., 2014).

(Figure 1). The Yusuf fault acted therefore as a buttress separating two areas with contrasting styles of extension: the radial pattern of rifting along the western and central Alboran Sea and the SW-NE extension to the east, which affects the transitional magmatic crust in the EAB and links to the SW-NE to W-E opening of the oceanic Algerian Basin.

## 9.2. Postrift Partial Inversion and Controlling Factors

Tectonic inversion and strike-slip faulting occurred in the Alboran Sea Basin from the latest Tortonian to present day (Bourgeois et al., 1992; Comas et al., 1992, 1999; Woodside & Maldonado, 1992), when the renewed NW-SE African/Eurasian plate-convergence became dominant and produced ~50 km of shortening (Jolivet & Faccenna, 2000; Morel & Meghraoui, 1996; Rosenbaum et al., 2002). Our results show that this inversion was partial and varied through space and time. Partial positive tectonic inversion took place along the Habibas Basin and EAB during the late Tortonian to Pliocene (Figures 9 and 13; R3 to p2), but most of the inversion was concentrated along the Alboran Ridge from early Pliocene to present day (Figures 7, 8, and 14a). This event is evident in the central and western parts of the ridge, where shortening produced reactivation of some SW-NE Miocene faults and anticline folding. To the west of our study area, El-Jebha well penetrated a similar uplifted and folded Miocene depocentre with thin Pliocene sequences on top forming the Xauen Bank offshore of Morocco, which is the southwestern prolongation of the Alboran Ridge (Figure 1; Bourgeois et al., 1992; Do Couto et al., 2016). Thus, the Xauen Bank and the western Alboran Ridge were probably part of the same subsiding Miocene depocentre that became an uplifting high. The Miocene sequence in the El-Jebha well contains several overpressure levels that accommodated part of the shortening resulting in shale tectonics in the WAB, which is coeval with the Plio-Quaternary uplift of the Alboran Ridge to the east. In addition, our findings demonstrate that the SSW-NNE trending Al-Idrisi fault that marks the boundary between the Alboran Ridge and Xauen Bank is another example of tectonic inheritance. At least the southern segment of the Al-Idrisi fault is a partially inverted Miocene structure producing syn-sedimentary uplift since the Messinian, being therefore an older structure than previously considered (Figure 5) (Grevemeyer et al., 2015; Martínez-García, Soto, & Comas, 2011). Inversion of Miocene normal faults has also been reported on the Moroccan margin occurring at a similar time mainly along the Bokkoya fault (Figure 1) (Chalouan et al., 1997; d'Acremont et al., 2014). Some Miocene extension-related structures in the WAB were also reactivated and shortened during the Plio-Quaternary (Comas & Soto, 1999). All these observations suggest that although the Alboran Ridge and Xauen Bank accommodated most of the contraction during the late Pliocene, the inversion was more widely distributed.

The inverted structures along the Alboran Ridge and Habibas Basin are examples of classical positive inversion, where the fault reactivations produced a change of the dip-slip component from normal to reverse (Williams, Powell, & Cooper, 1989). In contrast, the reactivation of the Yusuf fault zone is more complicated and includes a lateral component of motion (Figure 16). The Plio-Quaternary right-lateral displacement along Yusuf fault is an expression of the NW-SE convergence of the African and Eurasian plates (e.g., Alvarez-Marrón, 1999; Mauffret et al., 2007; Willet, 1997; Woodside & Maldonado, 1992). Our results show that the Yusuf fault has an earlier history and formed during the Miocene rifting. Older normal fault planes were reactivated in the Plio-Quaternary with oblique-slip motion (Figure 11). Reactivation mainly occurred in the eastern sector of the fault zone, while new subvertical fault planes with minor normal components of displacement were generated at its westernmost part cutting previous Miocene depocentres (cf. Figures 6a and 6b, 10, and 11). The WNW-ESE Yusuf fault zone could have had a left-lateral transtensional movement accommodating the oblique migration of the Alboran Domain during the Miocene, and it changed to predominantly right-lateral at Plio-Quaternary times, once the westwards migration and extension finished and NW-SE shortening and inversion prevailed (Figure 16) (Bourgeois et al., 1992; Giaconia et al., 2015; Martínez-García et al., 2013; Strzeczynski et al., 2010; Yelles et al., 2009).

Figure 14 shows that tectonic inversion in Alboran was very localised as it only affected some fault segments from the extensive set of preexisting normal faults. The orientation of the Miocene normal faults with respect to the renewed NW-SE Africa/Eurasia plate convergence vector seems to be a major controlling factor on which faults were reactivated. Those that accommodated the inversion are faults either subperpendicular or oblique to subparallel to the convergence vector and reactivated in either a reverse (i.e., Alboran Ridge and Habibas) or strike-slip (i.e., Yusuf fault) sense. Nevertheless, other factors must have played a



significant role as only some of the favourably oriented SW-NE Miocene faults were reactivated and new faults and folds were also formed (Figure 6).

Sandbox analogue modelling and field studies reveal that the dip of the original normal faults is also an important factor controlling inversion (e.g., Dart, McClay, & Hollings, 1995; Eisenstadt & Withjack, 1995; Marques & Nogueira, 2008). One of the most obvious features of depth-converted sections in Figure 15 is how variable the dips of Miocene normal faults are (15–65°). During the first stages of crustal extension in Alboran, all these faults must have had the typical high-angle of normal faults (55–65°), but with continued extension, sets of normal faults dipping in the same direction and their intervening fault blocks may rotate progressively to lower dips in a domino-like manner (e.g., Mandl, 1987). Then, the lowest dipping faults in a rotated set may be preferentially reactivated in compression (e.g., Bonini, Sani, & Antonielli, 2012; Kelly et al., 1999; Sibson, 1995). The structure observed along the EAB, where Tortonian to Pliocene anticlines are spatially linked to underlying normal faults comprising uplifted and folded Miocene thickening syn-rift wedges (Figures 9 and 15c, SP 2,400 and 3,300, top basement to p3 reflectors), is consistent with these mechanisms that explain the onset of inversion in the central part of the basin coinciding with areas of greatest former extension. Although we cannot be sure that the major reverse fault to the north of the Alboran Ridge was active before the Messinian, it is possible that this is another Miocene inverted normal fault forming part of the same set of south-dipping faults. All the inverted normal faults in the Alboran Ridge have listric geometries (Figures 7–9). Similar observations can be made for the partially inverted structures of the Al-Idrisi fault and Habibas Basin (Figures 5 and 13). It suggests that the listric geometry of some normal faults favoured their reactivation in compression due to their low dip at deeper structural levels similarly to the behaviour predicted by experimental models (e.g., Bonini et al., 2012; Eisenstadt & Withjack, 1995). For faults of low dip, preferential fault reactivation occurs where fluid pressure levels are locally elevated. Thus, the location of the thickest accumulation of sediments, where fluid content is likely to be greatest, provides another mechanism of selective reactivation (e.g., Kelly et al., 1999; Sibson, 1995). This may explain that most of the inversion in Alboran occurs along the Alboran Ridge and the Habibas half-graben where listric faults and thick depocentres coincide (Figures 6, 7, and 13).

The role of rheological anisotropies in the continental basement is also likely to be important. Inversion and reactivation only continued until the present day in areas that experienced young volcanism, for example, along the Alboran Ridge and Yusuf fault zones, where volcanic rocks intruded at 9.4–9.6 Ma and ~10.7 Ma, respectively (e.g., Duggen et al., 2004; Hoernle et al., 1999). The large curved magnetic anomaly along the central part of the basin marks the location of the Tortonian magmatic province, probably coinciding with the axis of greatest Miocene extension (Figure 14b). Therefore, these magmatic intrusions represent a prominent crustal heterogeneity that helped to focus stress leading to preferential tectonic inversion and strike-slip reactivation (Figure 16).

## 10. Conclusions

1. Normal faults, tilted blocks of basement, and syn-rift Miocene growth wedges document Miocene extension with a predominant NW-SE trend in the central and southeastern Alboran Sea. The WNW-ESE Yusuf zone acted as a buttress between the continental rifting in Alboran and a secondary SW-NE trend of extension affecting the transitional crust of the EAB that links to the oceanic spreading of the Algerian Basin.
2. The preserved Miocene depocentres in the central and southeastern Alboran, where the oldest deposits are of probable Serravallian age, are younger and thinner than those in the western and northern parts of the basin (2.5–3.5 km in the EAB versus up to 6 km in the WAB). Rifting finished at mid-Tortonian in the WAB, EAB, and Habibas Basin. Abundant volcanic rocks were intruded along the Alboran Ridge and Yusuf fault zones between ~9.4 Ma and ~10.7 Ma in the basin centre, where crustal thinning was greatest.
3. Post-Tortonian NW-SE shortening produced tectonic inversion distributed in time and space along the Habibas Basin and the Alboran Ridge, Yusuf, and Al-Idrisi faults. Inversion was partial, and some reactivated faults are still in net extension. Complete, positive, inversion occurred along the Alboran Ridge since the latest Tortonian to present day and a major uplift episode culminated at ~2.45 Ma. The Yusuf fault was also partially reactivated at a similar time, but with an additional component of strike-slip motion generating transpressional structures.

4. A number of factors controlled the selective tectonic inversion: (1) orientation of the Miocene normal faults with respect to the Plio-Quaternary NW-SE Africa/Eurasia plate convergence vectors; (2) original dips and geometries of Miocene faults; (3) higher fluid content along the thickest sedimentary accumulations; and (4) abundant magmatic intrusions along the Alboran Ridge and Yusuf fault zones helped to focus recent deformation at prominent rheological boundaries.

## Acknowledgments

This research was financed by the Projects CTM2009-057715/MAR (GASALB), CGL2008-03474-E/BTE (TOPOMED), Consolider-Ingenio 2010 CSD2006-00041 (TOPO-IBERIA) from R&D Plan MICINN and FEDER Funds, Spain, the Research Group RNM-215 (PAI Junta de Andalucía, Spain), and the Spanish program of Itinerario Integrado de Inserción Profesional (I3P form CSIC). We are grateful to J.I. Soto for his huge contribution to this research and fruitful discussions. IHS is acknowledged for the Kingdom Suite<sup>®</sup> software educational license. P.M.G. was hosted at Imperial College London, funded by a Spanish government mobility allowance for part of this work. Seismic and well data are available at the Archivo Técnico de Hidrocarburos (<https://geoportal.mine-tur.gob.es/ATHv2/welcome.do>). We thank P. Münch, two anonymous reviewers, and the Editor Claudio Faccenna for their constructive comments.

## References

- Achalhi, M., Münch, P., Cornée, J. J., Azdimousa, A., Melinte-Dobrinescu, M., Quillévéré, F., ... Feddi, N. (2016). The late Miocene Mediterranean-Atlantic connections through the North Rifian Corridor: New insights from the Boudinar and Arbaa Taourirt basins (northeastern Rif, Morocco). *Palaeogeography, Palaeoclimatology, Palaeoecology*, 459, 131–152.
- d'Acremont, E., Gutscher, M. A., Rabaute, A., Mercier De Lépinay, B., Lafosse, M., Poort, J., ... Gorini, C. (2014). High-resolution imagery of active faulting offshore Al Hoceima, Northern Morocco. *Tectonophysics*, 632, 160–166.
- Alonso, B., Ercilla, G., Martínez-Ruiz, F., Baraza, J., & Galimont, A. (1999). Pliocene-Pleistocene sedimentary facies at site 976: depositional history in the northwestern Alboran Sea. In R. Zahn, et al. (Eds.), *Proceedings ODP, Scientific Results*, 161 (pp. 57–68). College Station, TX: Ocean Drilling Program.
- Alonso, B., & Maldonado, A. (1992). Plio-Quaternary margin growth pattern in a complex tectonic setting: Northeastern Alboran Sea. *Geo-Marine Letters*, 12, 137–143.
- Alvarez-Marrón, J. (1999). Pliocene to Holocene structure of the eastern Alboran Sea (western Mediterranean). In R. Zahn, et al. (Eds.), *Proc. ODP, Scientific Results*, 161 (pp. 345–355). College Station, TX: Ocean Drilling Program.
- Ammar, A., Mauffret, A., Gorini, C., & Jabour, H. (2007). The tectonic structure of the Alboran margin of Morocco. *Sociedad Geológica de España*, 20, 247–271.
- Andrieux, J., Fontbote, J. M., & Mattauer, M. (1971). Sur un modele explicatif de l'arc de Gibraltar. *Earth and Planetary Science Letters*, 12(2), 191–198.
- Azdimousa, A., & Bourgois, J. (1993). Les communications entre l'Atlantique et la Méditerranée par le couloir sud-rifain du Tortonien à l'actuel: Stratigraphie séquentielle des bassins néogènes de la région du cap des Trois Fourches (Rif Oriental, Maroc). *Journal of African Earth Sciences*, 17(2), 233–240.
- Azdimousa, A., Jabaloy, A., Asebriy, L., Booth-Rea, G., González-Lodeiro, F., & Bourgois, J. (2007). Lithostratigraphy and structure of the Tamsamane unit (Eastern External Rif, Morocco). *Revista de la Sociedad Geológica de España*, 20(3–4), 187–200.
- Balanyá, J. C., & García-Dueñas, V. (1987). Les directions structurales dans le Domaine d'Alboran de parts et d'autre du Détroit de Gibraltar. *Comptes Rendus de l'Académie des Sciences Paris*, 304, 929–933.
- Benmakhlouf, M., Galindo-Zaldívar, J., Chalouan, A., Sanz de Galdeano, C., Ahmamou, M., & López-Garrido, A. C. (2012). Inversion of transfer faults: The Jebha-Chrafate fault (Rif, Morocco). *Journal of African Earth Sciences*, 73–74, 33–43.
- Bonini, M., Sani, F., & Antonielli, B. (2012). Basin inversion and contractional reactivation of inherited normal faults: A review based on previous and new experimental models. *Tectonophysics*, 522–523, 55–88.
- Booth-Rea, G., Jabaloy-Sánchez, A., Azdimousa, A., Asebriy, L., Vilchez, M. V., & Martínez-Martínez, J. M. (2012). Upper-crustal extension during oblique collision: The Tamsamane extensional detachment (eastern Rif, Morocco). *Terra Nova*, 24(6), 505–512.
- Bourgois, J., Mauffret, A., Ammar, A., & Demnati, A. (1992). Multichannel seismic data imaging of inversion tectonics of the Alboran Ridge (western Mediterranean Sea). *Geo-Marine Letters*, 12, 117–122.
- Butler, R. W. H. (1989). The influence of pre-existing basin structure on thrust system evolution in the Western Alps. *Geological Society London, Special Publications*, 44(1), 105–122.
- Calvert, A., Sandvol, E., Seber, D., Barazangi, M., Roecker, S., Mourabit, T., ... Jabour, N. (2000). Geodynamic evolution of the lithosphere and upper mantle beneath the Alboran Region of the western Mediterranean: Constraints from travel time tomography. *Journal of Geophysical Research*, 105(B5), 10,871–10,898. <https://doi.org/10.1029/2000JB900024>
- Carrera, N., Muñoz, J. A., Sábato, F., Mon, R., & Roca, E. (2006). The role of inversion tectonics in the structure of the Cordillera Oriental (NW Argentinean Andes). *Journal of Structural Geology*, 28(11), 1921–1932.
- Catalano, R., Franchino, A., Merlini, S., & Sulli, A. (2000). A crustal section from the Eastern Algerian basin to the Ionian Ocean (Central Mediterranean). *Memorie della Società Geologica Italiana*, 55, 71–85.
- Chalouan, A., & Michard, A. (2004). The Alpine Rif Belt (Morocco): A case of mountain building in a subduction-subduction-transform fault triple junction. *Pure and Applied Geophysics*, 161, 489–519.
- Chalouan, A., Michard, A., El Kadiri, K., Negro, F., Frizon de Lamotte, D., Soto, J. I., & Saddiqi, O. (2008). The Rif Belt. In A. Michard, et al. (Eds.), *The Rif Belt Continental Evolution: The Geology of Morocco. Structure, Stratigraphy, and Tectonics of the Africa-Atlantic-Mediterranean Triple Junction. Lecture in Earth Sciences* (pp. 203–302). Berlin: Springer.
- Chalouan, A., Saji, R., Michard, A., & Bally, A. W. (1997). Neogene tectonic evolution of the southwestern Alboran Basin as inferred from seismic data off Morocco. *American Association of Petroleum Geologists Bulletin*, 81(7), 1161–1184.
- Clauzon, G., Suc, J. P., Gautier, F., Berger, A., & Loutre, M. F. (1996). Alternate interpretation of the Messinian Salinity Crisis: Controversy resolved? *Geology*, 24(4), 363–366.
- Cloetingh, S., Beekman, F., Van Wees, J. D., Ziegler, P. A., & Sokoutis, D. (2008). Post-rift compressional reactivation potential of passive margins and extensional basins. In E. A. H. Johnson (Eds.), *The Nature and Origin of Compression in Passive Margins* (pp. 27–70). London: Geological Society London, Special Publications.
- Cohen, K. M., Finney, S. C., Gibbard, P. L., & Fan, J. X. (2013). The ICS international chronostratigraphic chart, Episodes. *International Commission on Stratigraphy*, 36(3), 199–204.
- Comas, M. C., García-Dueñas, V., & Jurado, M. J. (1992). Neogene tectonic evolution of the Alboran Sea from MCS data. *Geo-Marine Letters*, 12, 157–164.
- Comas, M. C., Platt, J. P., Soto, J. I., & Watts, A. B. (1999). The origin and tectonic history of the Alborán Basin: Insights from Leg 161 results. In R. Zahn, et al. (Eds.), *Proceedings ODP, Scientific Results*, 161 (pp. 555–579). College Station, TX: Ocean Drilling Program.
- Comas, M. C., & Soto, J. I. (1999). Brittle deformation in the metamorphic basement at site 976: Implications for middle Miocene extensional tectonics in the western Alboran basin. In R. Zahn, et al. (Eds.), *Proceedings of the Ocean Drilling Program, Scientific Results*, 161 (pp. 331–344). College Station, TX: Ocean Drilling Program.
- Cornée, J. J., Münch, P., Achalhi, M., Merzeraud, G., Azdimousa, A., Quillévéré, F., ... Moissette, P. (2016). The Messinian erosional surface and early Pliocene reflooding in the Alboran Sea: New insights from the Boudinar basin, Morocco. *Sedimentary Geology*, 333, 115–129.



- Dart, C. J., McClay, K., & Hollings, P. N. (1995). 3D analysis of inverted extensional fault systems, southern Bristol Channel basin, UK. In J. G. Buchanan, & P. G. Buchanan (Eds.), *Basin Inversion* (pp. 393–413). London: Geological Society London, Special Publications.
- Dewey, J. F. (1988). Extensional collapse of orogens. *Tectonics*, 7, 1123–1139. <https://doi.org/10.1029/TC0071006p01123>
- Do Couto, D., Gorini, C., Jolivet, L., Lebre, N., Augier, R., Gumiaux, C., ... Auxietre, J. L. (2016). Tectonic and stratigraphic evolution of the Western Alboran Sea Basin in the last 25 Myrs. *Tectonophysics*, 677–678, 280–311.
- Docherty, C., & Banda, E. (1995). Evidence for the eastward migration of the Alboran Sea based on regional subsidence analysis: A case for basin formation by delamination of the subcrustal lithosphere. *Tectonics*, 14(4), 804–818. <https://doi.org/10.1029/95TC00501>
- Domzig, A., Yelles, K., Le Roy, C., Déverchère, J., Bouillin, J. P., Bracène, R., ... Pauc, H. (2006). Searching for the Africa-Eurasia Miocene boundary offshore western Algeria (MARADJA'03 cruise). *Comptes Rendus Geosciences*, 338(1–2), 80–91.
- Duggen, S., Hoernle, K., van den Bogaard, P., & Harris, C. (2004). Magmatic evolution of the Alboran region: The role of subduction in forming the western Mediterranean and causing the Messinian Salinity Crisis. *Earth and Planetary Science Letters*, 218(1–2), 91–108.
- Eisenstadt, G., & Withjack, M. O. (1995). Estimating inversion: Results from clay models. *Geological Society London, Special Publications*, 88(1), 119–136.
- Faccenna, C., Piromallo, C., Crespo-Blanc, A., Jolivet, L., & Rossetti, F. (2004). Lateral slab deformation and the origin of the western Mediterranean arcs. *Tectonics*, 23, TC1012. <https://doi.org/10.1029/2002TC001488>
- Frizon de Lamotte, D., Andrieux, J., & Guézou, J. C. (1991). Cinématique des chevauchements Néogènes dans l'arc Bético-Rifain: Discussion sur les modèles géodynamiques. *Bulletin de la Société Géologique de France*, 4, 611–626.
- Galdeano, A., Courtillot, V., Le Borgne, E., Le Mouél, J. L., & Rossignol, J. C. (1974). An aeromagnetic survey of the southwest of the western Mediterranean: Description and tectonic implications. *Earth and Planetary Science Letters*, 23, 323–336.
- Galindo-Zaldívar, J., Azzouz, O., Chalouan, A., Pedrera, A., Ruano, P., Ruiz-Constán, A., ... Benmakhoulou, M. (2015). Extensional tectonics, graben development and fault terminations in the eastern Rif (Bokoya-Ras Afraou area). *Tectonophysics*, 663, 140–149.
- Galindo-Zaldívar, J., González Lodeiro, F., & Jabaloy, A. (1989). Progressive extensional shear structures in a detachment contact in the Western Sierra Nevada (Betic Cordilleras, Spain). *Geodinamica Acta*, 3, 73–85.
- Gallais, F., Gutscher, M. A., Graindorge, D., Chamot-Rooke, N., & Klaeschen, D. (2011). A Miocene tectonic inversion in the Ionian Sea (central Mediterranean): Evidence from multichannel seismic data. *Journal of Geophysical Research*, 116, B12108. <https://doi.org/10.1029/2011JB008505>
- García-Dueñas, V., Balanyá, J. C., & Martínez-Martínez, J. M. (1992). Miocene extensional detachments in the outcropping basement of the northern Alboran basin (Betics) and their tectonic implications. *Geo-Marine Letters*, 12, 88–95.
- Giaconia, F., Booth-Rea, G., Ranero, C. R., Gràcia, E., Bartolome, R., Calahorrano, A., ... Viñas, M. (2015). Compressional tectonic inversion of the Algero-Balearic basin: Latest Miocene to present oblique convergence at the Palomares margin (western Mediterranean). *Tectonics*, 34, 1516–1543. <https://doi.org/10.1002/2015TC003861>
- Grevenmeyer, I., Gràcia, E., Villaseñor, A., Leuchters, W., & Watts, A. B. (2015). Seismicity and active tectonics in the Alboran Sea, western Mediterranean: Constraints from an offshore-onshore seismological network and swath bathymetry data. *Journal of Geophysical Research: Solid Earth*, 120, 8348–8365. <https://doi.org/10.1002/2015JB012073>
- Gutscher, M. A., Malod, J., Rehault, J. P., Contrucci, I., Klingelhoefer, F., Mendes, V. L., & Spakman, W. (2002). Evidence for active subduction beneath Gibraltar. *Geology*, 30(12), 1071–1074.
- Hanne, D., White, N., & Lonergan, L. (2003). Subsidence analyses from the Betic Cordillera, Southeast Spain. *Basin Research*, 15, 1–21.
- Hayward, A. B., & Graham, R. H. (1989). Some geometrical characteristics of inversion. *Geological Society London, Special Publications*, 44(1), 17–39.
- Hoernle, K., van den Bogaard, P., Duggen, S., Mocek, B., & Garbe-Schönberg, D. (1999). Evidence for Miocene subduction beneath the Alboran Sea: 40AR/39AR dating and geochemistry of volcanic rocks from holes 977A and 978A1. In R. Zahn, et al. (Eds.), *Proceedings ODP, Scientific Results*, 161 (pp. 357–373). College Station, TX: Ocean Drilling Program.
- Horvath, F., & Berckhemer, H. (1982). Mediterranean backarc basins. In H. Berckhemer & K. Hsü (Eds.), *Alpine Mediterranean Geodynamics* (pp. 141–173). Washington, DC: American Geophysical Union.
- Hsü, K. J., Ryan, W. B. F., & Cita, M. B. (1973). Late Miocene desiccation of the Mediterranean. *Nature*, 242(5395), 240–244.
- Iaccarino, S. M., & Bossio, A. (1999). Paleoenvironment of uppermost Messinian sequences in the western Mediterranean (Sites 974, 975, and 978). In R. Zahn, et al. (Eds.), *Proceedings of the Ocean Drilling Program, Scientific Results*, 161 (pp. 529–541). College Station, TX: Ocean Drilling Program.
- Iribarren, L., Vergés, J., & Fernández, M. (2009). Sediment supply from the Betic-Rif orogen to basins through Neogene. *Tectonophysics*, 475(1), 68–84.
- Jackson, C. A. L., & Larsen, E. (2008). Temporal constraints on basin inversion provided by 3D seismic and well data: A case study from the South Viking Graben, offshore Norway. *Basin Research*, 20(3), 397–417.
- Jackson, J. A. (1980). Reactivation of basement faults and crustal shortening in orogenic belts. *Nature*, 283(5745), 343–346.
- Jolivet, L., & Faccenna, C. (2000). Mediterranean extension and the Africa-Eurasia collision. *Tectonics*, 19(6), 1095–1106. <https://doi.org/10.1029/2000TC900018>
- Jones, R. R., Holdsworth, R. E., Clegg, P., McCaffrey, K., & Tavarnelli, E. (2004). Inclined transpression. *Journal of Structural Geology*, 26(8), 1531–1548.
- Juan, C., Ercilla, G., Hernández-Molina, J., Estrada, F., Alonso, B., Casas, D., ... Ammar, A. (2016). Seismic evidence of current-controlled sedimentation in the Alboran Sea during the Pliocene and Quaternary: Palaeoceanographic implications. *Marine Geology*, 378, 292–311.
- Jurado, M. J., & Comas, M. C. (1992). Well log interpretation and seismic character of the Cenozoic sequence in the northern Alboran Sea. *Geo-Marine Letters*, 12, 129–136.
- de Kaenel, E. P., Siesser, W. G., & Murat, A. (1999). Pleistocene calcareous nannofossil biostratigraphy and the western Mediterranean sapropels, sites 974 to 977 and 979. In R. Zahn, et al. (Eds.), *Proceedings of the Ocean Drilling Program, Scientific Results*, 161 (pp. 159–183). College Station, TX: Ocean Drilling Program.
- Kelly, P. G., Peacock, D. C. P., Sanderson, D. J., & McGurk, A. C. (1999). Selective reverse-reactivation of normal faults, and deformation around reverse-reactivated faults in the Mesozoic of the Somerset coast. *Journal of Structural Geology*, 21(5), 493–509.
- Kheidri, L. H., Benabdelmounen, M. S., & Zazoun, R. S. (2000). Evolution structurale de la partie orientale du bassin d'Alboran au cours du Néogène (offshore occidentale, Algérie). In F. Briand (Ed.), *African Continental Margin of the Mediterranean Sea, CIESM Workshop Series* (pp. 40–43). Djerba, Tunisia: CIESM.
- Krijgsman, W., Hilgen, F. J., Raffi, I., Sierro, F. J., & Wilson, D. S. (1999). Chronology, causes and progression of the Messinian salinity crisis. *Letters to Nature*, 400, 652–655.

- Le Gall, B., Vétel, W., & Morley, C. K. (2005). Inversion tectonics during continental rifting: The Turkana Cenozoic rifted zone, northern Kenya. *Tectonics*, 24, TC2002. <https://doi.org/10.1029/2004TC001637>
- Leprêtre, A., Klingelhoefer, F., Graindorge, D., Schnurle, P., Beslier, M. O., Yelles, K., ... Déverchère, J. (2013). Multiphased tectonic evolution of the Central Algerian margin from combined wide-angle and 2D reflection seismic data off Tipaza, Algeria. *Journal of Geophysical Research: Solid Earth*, 118, 3899–3916. <https://doi.org/10.1002/jgrb.50318>
- Loneragan, L., Platt, J. P., & Gallagher, L. (1994). The internal-external zone boundary in the eastern Betic Cordillera, SE Spain. *Journal of Structural Geology*, 16, 175–188.
- Loneragan, L., & White, N. (1997). Origin of the Betic-Rif mountain belt. *Tectonics*, 16(3), 504–522. <https://doi.org/10.1029/96TC03937>
- Maldonado, A., Campillo, A. C., Mauffret, A., Alonso, B., Woodside, J., & Campos, J. (1992). Alboran Sea Late Cenozoic tectonic and stratigraphic evolution. *Geo-Marine Letters*, 12, 179–186.
- Mandl, G. (1987). Tectonic deformation by rotating parallel faults: The “bookshelf” mechanism. *Tectonophysics*, 141(4), 277–316.
- Marques, F. O., & Nogueira, C. R. (2008). Normal fault inversion by orthogonal compression: Sandbox experiments with weak faults. *Journal of Structural Geology*, 30(6), 761–766.
- Martínez-García, P., Comas, M., Soto, J. I., Lonergan, L., & Watts, A. B. (2013). Strike-slip tectonics and basin inversion in the Western Mediterranean: The Post-Messinian evolution of the Alboran Sea. *Basin Research*, 25(4), 361–387.
- Martínez-García, P., Soto, J. I., & Comas, M. (2011). Recent structures in the Alboran Ridge and Yusuf fault zones based on swath bathymetry and sub-bottom profiling: Evidence of active tectonics. *Geo-Marine Letters*, 31, 16–39.
- Martínez-Martínez, J. M., & Azañón, J. M. (1997). Mode of extensional tectonics in the southeastern Betics (SE Spain): Implications for the tectonic evolution of the peri-Alborán orogenic system. *Tectonics*, 16(5–6), 205–225. <https://doi.org/10.1029/97TC00157>
- Martínez-Martínez, J. M., Soto, J. I., & Balanyá, J. C. (2004). Elongated domes in extended orogens: A mode of mountain uplift in the Betics (SE Spain). In D. L. Whitney, C. Teyssier, & C. S. Siddoway (Eds.), *Gneiss Domes in Orogeny* (pp. 243–265). Boulder, CO: Geological Society of America.
- Mauffret, A. (2007). The northwestern (Maghreb) boundary of the Nubia (Africa) Plate. *Tectonophysics*, 429, 21–44.
- Mauffret, A., Ammar, A., Gorini, C., & Jabour, H. (2007). The Alboran Sea (western Mediterranean) revisited with a view from the Moroccan Margin. *Terra Nova*, 19(3), 195–203.
- Mauffret, A., Frizon-de-Lamotte, D., Lallemand, S., Gorini, C., & Maillard, A. (2004). E-W opening of the Algerian Basin (western Mediterranean). *Terra Nova*, 16, 257–264.
- McClay, K. R., & Anderton, R. (1989). Inversion of the Kechika Trough, Northeastern British Columbia, Canada. *Geological Society London, Special Publications*, 44(1), 235–257.
- Medaouri, M., Déverchère, J., Graindorge, D., Bracene, R., Badji, R., Ouabadi, A., ... Bendiab, F. (2014). The transition from Alboran to Algerian basins (western Mediterranean Sea): chronostratigraphy, deep crustal structure and tectonic evolution at the rear of a narrow slab rollback system. *Journal of Geodynamics*, 77, 186–205.
- Molnar, P., & Houseman, G. A. (2004). The effects of buoyant crust on the gravitational instability of thickened mantle lithosphere at zones of intracontinental convergence. *Geophysical Journal International*, 158(3), 1134–1150.
- Morel, J. L., & Meghraoui, M. (1996). Goringe-Alboran-Tell tectonic zone: A transpression system along the Africa-Eurasia plate boundary. *Geology*, 24, 755–758.
- Morley, C. K. (1993). Discussion of origins of hinterland basins to the Rif-Betic Cordillera and Carpathians. *Tectonophysics*, 226(1), 359–376.
- Munteanu, I., Matenco, L., Dinu, C., & Cloetingh, S. (2011). Kinematics of back-arc inversion of the Western Black Sea Basin. *Tectonics*, 30, TC5004. <https://doi.org/10.1029/2011TC002865>
- Pérez-Belzuz, F., Alonso, B., & Ercilla, G. (1997). History of mud diapirism and triggering mechanisms in the Western Alboran Sea. *Tectonophysics*, 282, 399–423.
- Platt, J. P., Soto, J. I., Whitehouse, M. J., Hurford, A. J., & Kelley, S. P. (1998). Thermal evolution, rate of exhumation, and tectonic significance of metamorphic rocks from the floor of the Alboran extensional basin, Western Mediterranean. *Tectonics*, 17(5), 671–689. <https://doi.org/10.1029/98TC02204>
- Platt, J. P., & Vissers, R. L. M. (1989). Extensional collapse of thickened continental lithosphere: A working hypothesis for the Alboran Sea and Gibraltar Arc. *Geology*, 17, 540–543.
- Poujol, A., Ritz, J. F., Tahayt, A., Vernant, P., Condomines, M., Blard, P. H., ... Idrissi, A. K. (2014). Active tectonics of the Northern Rif (Morocco) from geomorphic and geochronological data. *Journal of Geodynamics*, 77, 70–88.
- Rehault, J. P., Boillot, G., & Mauffret, A. (1984). The western Mediterranean Basin geological evolution. *Marine Geology*, 55, 447–477.
- Rosenbaum, G., Lister, G. S., & Duboz, C. (2002). Relative motions of Africa, Iberia and Europe during Alpine orogeny. *Tectonophysics*, 359(1–2), 117–129.
- Royden, L. H. (1993). Evolution of retreating subduction boundaries formed during continental collision. *Tectonics*, 12, 629–638. <https://doi.org/10.1029/92TC02641>
- Ryan, W. B. F., Hsü, K. J., Cita, M. B., Dumitrica, P., Lort, J., Maync, W., ... Wezae, F. C. (1973). Western Alboran Basin-Site 121. In W. B. F. Ryan & K. J. Hsü (Eds.), *Initial Reports of the Deep Sea Drilling Project* (pp. 43–89). Washington, DC: Government Printing Office.
- Seber, D., Barazangi, M., Ibenbrahim, A., & Demnati, A. (1996). Geophysical evidence for lithospheric delamination beneath the Alboran Sea and Rif-Betics mountains. *Nature*, 379, 785–790.
- Sibson, R. H. (1995). Selective fault reactivation during basin inversion: Potential for fluid redistribution through fault-valve action. In J. G. Buchanan & P. G. Buchanan (Eds.), *Basin Inversion (Special Publications, London)* (pp. 3–19). London: Geological Society.
- Siesser, W. G., & de Kaenel, E. P. (1999). Neogene calcareous nannofossils: Western Mediterranean biostratigraphy and paleoclimatology. In R. Zahn, et al. (Eds.), *Proceedings of the Ocean Drilling Program, Scientific Results*, 161 (pp. 223–237). College Station, TX: Ocean Drilling Program.
- Soto, J. I., Comas, M. C., & de la Linde, J. (1996). Espesor de sedimentos en la Cuenca de Alborán mediante una conversión sísmica corregida. *Geogaceta*, 20(2), 382–385.
- Soto, J. I., Fernández-Ibáñez, F., Talukder, A. R., & Martínez-García, P. (2010). Miocene shale tectonics in the northern Alboran Sea (western Mediterranean). In L. Wood (Ed.), *Shale Tectonics, AAPG Memoir* (Vol. 93, pp. 119–144). Tulsa, OK: AAPG.
- Soto, J. I., & Platt, J. P. (1999). Petrological and structural evolution of high-grade metamorphic rocks from the floor of the Alboran Sea Basin, western Mediterranean. *Journal of Petrology*, 40(1), 21–60.
- Strzeczynski, P., Déverchère, J., Cattaneo, A., Domzig, A., Yelles, K., de Lépinay, B. M., ... Boudiaf, A. (2010). Tectonic inheritance and Pliocene-Pleistocene inversion of the Algerian margin around Algiers: Insights from multibeam and seismic reflection data. *Tectonics*, 29, TC2008. <https://doi.org/10.1029/2009TC002547>
- Takano, O., Tateishi, M., & Endo, M. (2005). Tectonic controls of a backarc trough-fill turbidite system: The Pliocene Tamugigawa Formation in the Niigata-Shin'etsu inverted rift basin, Northern Fossa Magna, central Japan. *Sedimentary Geology*, 176(3–4), 247–279.



- Talukder, A.R. (2003). La Provincia Diapírica de lodo en la Cuenca Oeste del Mar de Alborán: Estructuras, Génesis y Evolución, (Doctoral thesis), University of Granada, Granada.
- Turner, J. P., & Williams, G. A. (2004). Sedimentary basin inversion and intra-plate shortening. *Earth-Science Reviews*, 65, 277–304.
- Turner, S. P., Platt, J. P., George, R. M. M., Kelley, S. P., Pearson, D. G., & Nowell, G. M. (1999). Magmatism associated with orogenic collapse of the Betic-Alboran Domain, SE Spain. *Journal of Petrology*, 40(6), 1011–1036.
- Watts, A. B., Platt, J. P., & Buhl, P. (1993). Tectonic evolution of the Alboran Sea basin. *Basin Research*, 5, 153–177.
- Weinzapfel, A. C., Mountfield, R. A., Chevalier, Y. M., Kuo, L. C., Soofi, K. A., Haddad, G. A., & Strickland, M. O. (2003). New insights into the hydrocarbon prospectivity of an undrilled mud diapir province, west Alboran Basin, Morocco-Spain: AAPG Annual Meeting, Abstract Book.
- Willet, A. (1997). Marine geophysical investigations of the Alboran Sea, (Doctoral thesis), Oxford University, Oxford.
- Williams, G. D., Powell, C. M., & Cooper, M. A. (1989). Geometry and kinematics of inversion tectonics. *Geological Society London, Special Publications*, 44(1), 3–15.
- Woodside, J. M., & Maldonado, A. (1992). Styles of compressional neotectonics in the Eastern Alboran Sea. *Geo-Marine Letters*, 12, 111–116.
- Yelles, A., Domzig, A., Déverchère, J., Bracène, R., Mercier de Lépinay, B., Strzeczynski, P., ... Djellit, H. (2009). Plio-Quaternary reactivation of the Neogene margin off NW Algiers, Algeria: The Khayr al Din bank. *Tectonophysics*, 475(1), 98–116.